Geologica Acta, Vol.8, N° 3, September 2010, 249-280
DOI: 10.1344/105.000001533
Available online at www.geologica-acta.com

geologica acta

Sedimentary evolution of an Aptian syn-rift carbonate system (Maestrat Basin, E Spain): effects of accommodation and environmental change

T. BOVER-ARNAL [1] J.A. MORENO-BEDMAR [2] R. SALAS [2] P.W. SKELTON [3] K. BITZER [1] E. GILI [4]

[1] **Abteilung Geologie, Fakultät für Biologie, Chemie und Geowissenschaften, Universität Bayreuth**
Universitätsstr, 30, 95440, Bayreuth, Germany. Bover-Arnal E-mail: Telm.Bover@uni-bayreuth.de

[2] **Departament de Geoquímica, Petrologia i Prospecció Geològica, Facultat de Geologia, Universitat de Barcelona**
Martí i Franqués s/n, 08028, Barcelona, Spain

[3] **Department of Earth and Environmental Sciences, The Open University**
Milton Keynes MK7 6AA, UK

[4] **Departament de Geologia, Facultat de Ciències, Universitat Autònoma de Barcelona**
Edifici Cs, 08193, Bellaterra (Cerdanyola del Vallès), Spain

ABSTRACT

We report an integrated study of an expanded and relatively complete syn-rift continental to epeiric marine succession of Aptian age, cropping out in the western Maestrat Basin (eastern Iberian Chain). Four transgressive-regressive sequences are recognized throughout this mixed carbonate-siliciclastic succession, with excellent age control provided by ammonite biostratigraphic data. The transgressive systems tracts consist mainly of alternations of marls and limestones rich in orbitolinids. The regressive systems tracts are essentially characterized by wave- and tidally influenced siliciclastic and carbonate deposits, and by the development of carbonate platforms with rudists, corals, orbitolinids and green algae. Carbon and oxygen isotope curves were established in order to identify the global $\delta^{13}C$ perturbations related to the Early Aptian Oceanic Anoxic Event (OAE1a). These perturbations commence with a horizon of coral rubble encrusted by *Lithocodium aggregatum* and *Bacinella irregularis* with widespread large-sized discoidal *Palorbitolina lenticularis*. Associated $\delta^{18}O$ values indicate high-frequency cooling-warming climatic cycles. The fault-controlled rapid syn-rift subsidence recorded during this stage was the most important factor in producing accommodation. However, the major transgressions, sea level falls and biotic changes recorded in the eastern Iberian Chain are in agreement with those registered in other contemporaneous basins of the Tethys. Thus, the resulting sedimentary succession faithfully reflects the major oceanographic and climatically-driven global changes that characterized this stage albeit within a context established by regional tectonics. Hence, this well-documented record of the evolution of an Aptian epicontinental sea provides a useful comparative case study for the analysis of other Aptian epeiric sedimentary successions.

KEYWORDS | Carbonate system. Sequence stratigraphy. OAE1a. Aptian. Iberian Chain.

INTRODUCTION

Many authors have characterized the Aptian as an eventful time with strong climatic changes ranging from greenhouse to sub-glacial conditions, a "superplume" volcanic episode in the Pacific Ocean, an oceanic anoxic event, significant eustatic variations, a platform crisis and turnover of marine biota (e.g., Weissert and Lini, 1991; Erba, 1994; Weissert et al., 1998; Menegatti et al., 1998; Larson and Erba, 1999; Hochuli et al., 1999; Pittet et al., 2002; Wissler et al., 2003; Skelton, 2003a; Weissert and Erba, 2004; Föllmi et al., 2006; Dumitrescu et al., 2006; Burla et al., 2008). In the Neo-Tethyan realm, large carbonate platforms dominated by rudists, corals, orbitolinids and green algae developed during this time (e.g., Malchus et al., 1996; Vilas et al., 1995; Rosales, 1999; Vennin and Aurell, 2001; Pittet et al., 2002; Hillgärtner et al., 2003; Millán et al., 2007; Bover-Arnal et al., 2008, 2009; Tomás et al., 2008). Platform carbonate producing biota are variously controlled by light, temperature, hydrodynamic conditions, basin-floor topography, seawater chemistry (O_2, CO_2, Mg, Ca, nutrients and salinity) and, over longer time intervals, eustasy (e.g., Hallock and Schlager, 1986; Pomar and Kendall, 2007). Hence, their observed ecological responses to changing external factors can be interpreted in terms of all these tectonically and climatically-driven events in the sedimentary record.

The Maestrat Basin (E Iberian Chain, Spain), especially the Galve sub-basin (western Maestrat Basin), offers an exceptional opportunity to study the interaction of these factors in a continuous and well-exposed continental to epicontinental marine succession that encompasses the entire Aptian Stage, with excellent time control based on ammonite biostratigraphy. To this end, the present work establishes a conceptual model that integrates the facies, sequence stratigraphy, carbon and oxygen isotopes, and quantitative subsidence analysis of the sedimentary succession.

Vennin and Aurell (2001) and Embry (2005) were the first to extensively document the sedimentary evolution of the Aptian succession in the Galve sub-basin. Vennin and Aurell (2001) performed facies and sequence stratigraphic analyses in the eastern part of the sub-basin. Embry (2005) revisited these sections and studied them in further detail, carrying out C- and O-isotope analyses and discussing palaeoenvironmental aspects of the platform carbonates. With this background, the present paper aims to further analyze and illustrate the sedimentary evolution of the Galve sub-basin. The inclusion of the central part of the sub-basin in the present study, together with the original data presented here, provide a more detailed and complete sub-basin-wide view of the Aptian Stage in this western margin of the Maestrat Basin. Moreover, alternative sequence stratigraphic and depositional models, different interpretations of the $\delta^{13}C$ and $\delta^{18}O$ curves, and extensive discussion of the tectonic and environmental factors controlling sedimentary evolution offer a revised global perspective. Recently, Bover-Arnal et al. (2009) carried out facies analysis and applied a four systems tract-based sequence stratigraphic method (see Hunt and Tucker, 1992) to the interpretation of late Early-Middle Aptian strata that were generated in the carbonate platform margin located in the central Galve sub-basin. The current paper, by contrast, analyzes the whole of the Aptian sedimentary succession throughout the Galve sub-basin in terms of transgressive-regressive (T-R) sequences (see Catuneanu et al., 2009).

The goals of the present study are: a) to show the relationship between tectonism, eustasy and evolution of this mixed carbonate-siliciclastic system; b) to investigate how these sensitive marine environments were affected by ocean-climate system perturbations; c) to contextualize the carbonate succession stratigraphically in order to establish similarities and differences with other Aptian carbonate systems developed along the Tethyan margins; and d) to provide an outstanding record of this stage that could serve to calibrate the analysis of other Aptian sedimentary successions. Furthermore, the implications concerning the roles of tectonics and eustasy in controlling accommodation, sequence stratigraphy, environmental change, carbonate platform evolution and carbon- and oxygen-isotope geochemistry are also of potential value for other non-Aptian studies.

STUDY AREA AND GEOLOGICAL SETTING

During Late Jurassic (Late Oxfordian) to Early Cretaceous (Middle Albian) times, the Iberian plate underwent extension due to the opening of the Central and North Atlantic domains. Rifting led to the formation of several intraplate basins in Iberia such as the Maestrat Basin. Later, as a result of the collision between the Iberian and European plates during the Alpine orogeny (Late Eocene to Early Miocene), the Iberian basins underwent tectonic inversion to form the Iberian Chain (Salas et al., 2001). The study area is located in the eastern Iberian Chain (E Spain) (Fig. 1A), between the villages of Campos, Camarillas and Villarroya de los Pinares, and the investigated succession crops out along two main Tertiary folds: the Camarillas syncline, striking NNE-SSW in the north and NNW-SSE in the south, and the Miravete anticline to the East of the latter, striking NNW-SSE (Fig. 1B). The area corresponds to the western margin of the Maestrat Basin known as the Galve sub-basin (Salas and Guimerà, 1996). Continental and marine carbonate and siliciclastic terrigenous sedimentation occurred in a context of differential subsidence with several half-graben structures related to synsedimentary ENE-WSW normal listric faulting. The latter were confined by steep NNW-SSE normal transfer faults (Fig. 1B) (Simón et al., 1998; Soria, 1997; Vennin and Aurell, 2001; Liesa et al., 2006). The Miravete fault

was a NNW-SSE Mesozoic normal transfer fault that partitioned the study area into a western, hanging-wall side, and an eastern, foot-wall side (Fig. 1B). This fault controlled facies architecture and thickness differences between the two sides (Simón et al., 1998).

The Aptian succession in the Galve sub-basin is up to 810 m thick, spans 13 Ma (the absolute age interval for the Aptian according to Ogg and Ogg, 2006), and is composed of five lithostratigraphic units with the rank of formations (Canérot et al., 1982). This stratigraphic record can be divided into four large-scale T-R sequences, the ages of which were calibrated with ammonite biostratigraphic data from the Galve sub-basin provided by Weisser (1959) and Moreno-Bedmar et al. (2009, accepted), geomagnetic polarity (Salas et al., 2005) and rudist biostratigraphy. The analyzed succession overlies a regional subaerial unconformity that separates Barremian marine mixed carbonate-siliciclastic sediments of the Artoles Formation below (Salas, 1987), from fluviatile deposits of the Morella Formation or terrigenous marine sediments of the lower part of the Xert Formation above (Fig. 2). The continental sediments of the Morella Formation are of earliest Aptian age (Salas et al., 2005) and become progressively more marine in character upwards in the succession. The four T-R sequences interpreted in this study comprise the last-

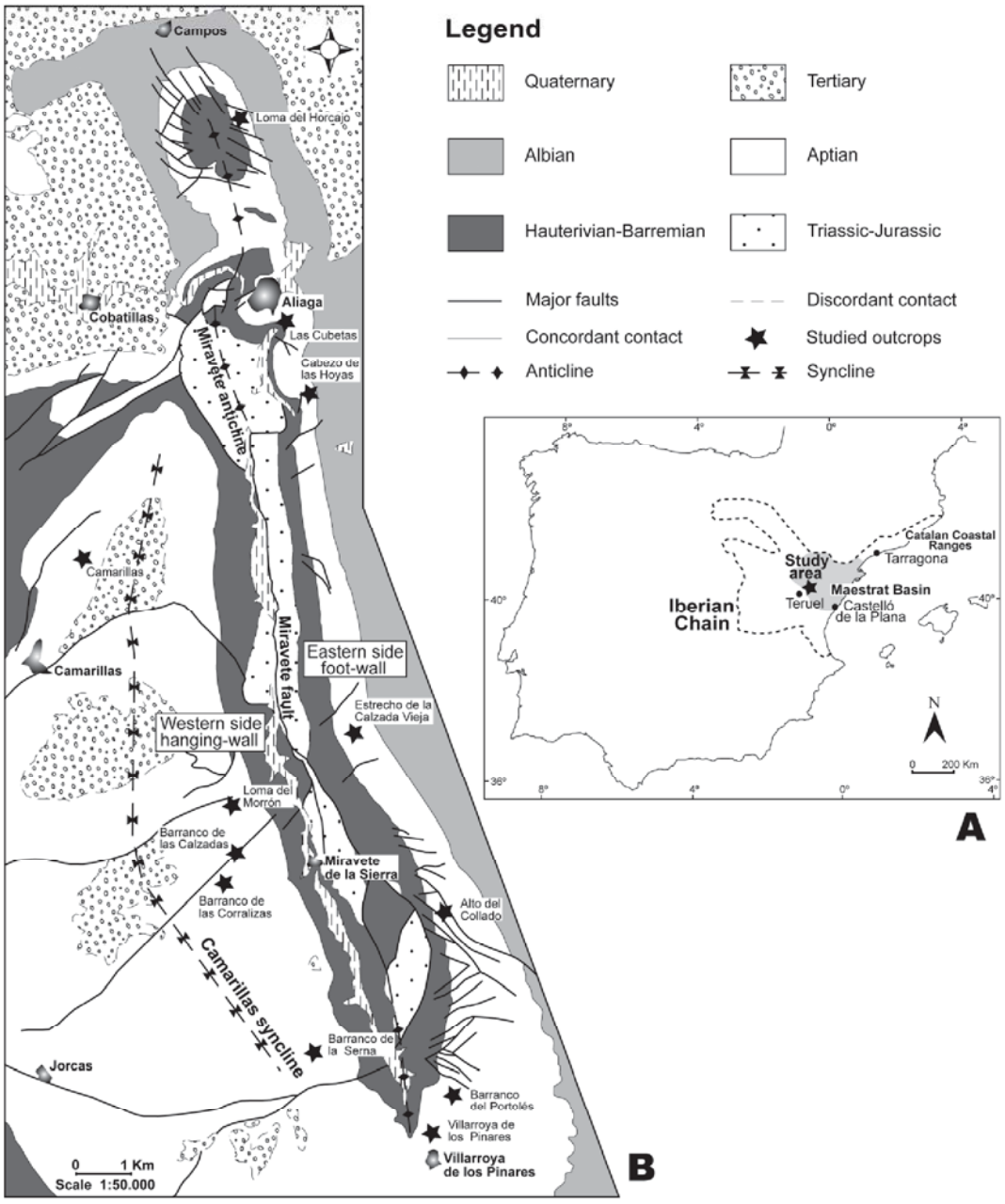

FIGURE 1 | **A) Geographical location of the study area in the eastern Iberian Chain (E-Spain). B) Geological setting and location of the studied outcrops. Modified after Canérot et al. (1979) and Gautier (1980).**

mentioned formation, and the Xert, Forcall, Villarroya de los Pinares and Benassal formations (Fig. 2). With the exception of the continental siliciclastic-rich earliest Aptian deposits, these sequences were produced in epeiric marine environments characterized by classical Tethyan Urgonian facies associations dominated by rudists, corals, green algae, orbitolinids and other benthic foraminifera. The top of the studied succession is marked by another regional unconformity (Fig. 2), which passes basinwards to a maximum regressive surface, and separates the transitional wave- and tidal-influenced sediments of the upper part of the Benassal Formation (below), from the carbon-rich deltaic deposits of the Escucha Formation (above). The base of this last-mentioned formation is of earliest Albian age (Moreno-Bedmar et al., 2008; Villanueva-Amadoz et al., 2008).

MATERIALS AND METHODS

Twelve well-exposed stratigraphic sections were measured along the Miravete anticline and Camarillas syncline. Five of them were logged on the east side of the Miravete fault (foot-wall), in Loma del Horcajo, Las Cubetas, Cabezo de las Hoyas, Estrecho de la Calzada Vieja and Alto del Collado. On the west side (hanging-wall), the remaining seven sections were logged in Camarillas, Loma del Morrón, Barranco de las Calzadas, Barranco de las Corralizas, Barranco de la Serna, Barranco del Portolés and Villarroya de los Pinares (Fig. 1B). A detailed sedimentological analysis was performed for each section. Microfacies were described from 166 thin sections of samples collected during field work.

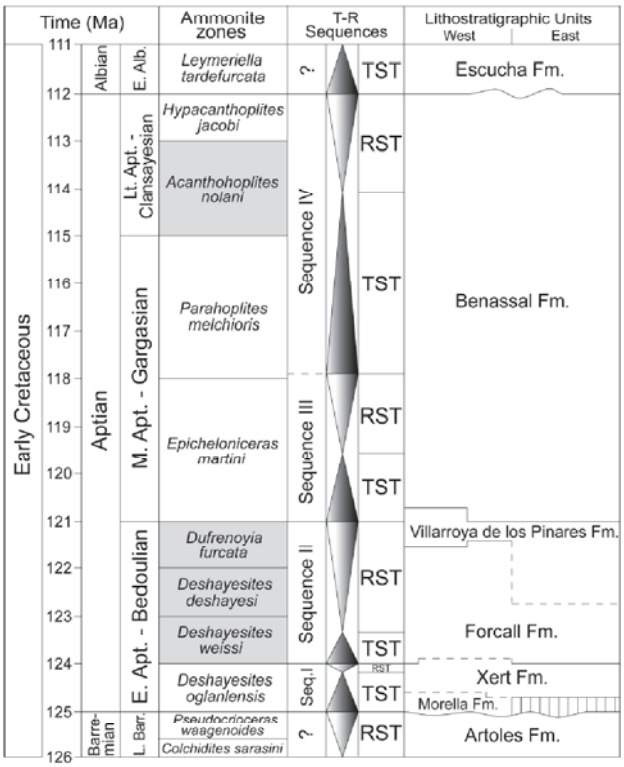

FIGURE 2 | **Stratigraphic framework and age relationships for the Aptian in the Galve sub-basin. Identified ammonite biozones are indicated in grey (Weisser, 1959; Moreno-Bedmar et al., 2009, accepted). Discontinuous lines indicate lack of absolute dating. Absolute ages are from Ogg and Ogg (2006). Modified from Bover-Arnal et al. (2009).**

The difficulty of recognizing lithostratigraphic surfaces with sequence stratigraphic significance *sensu* Van Wagoner et al. (1988) or Hunt and Tucker (1992) in most of the Aptian sedimentary succession studied here, has led us to adopt the approach of identifying T-R sequences (see Catuneanu et al., 2009). In exposed epicontinental carbonate sedimentary successions, the distinguishing physical characteristics of the three or four systems tract-based depositional sequences (Van Wagoner et al., 1988; Hunt and Tucker, 1992) are often masked or not preserved because of poor exposure conditions, variable rates of sediment production and accumulation, erosion or superimposition of surfaces. By contrast, the characterization of T-R sequences is mainly based on the recognition of surfaces that mark large-scale changes in trend from deepening- to shallowing-upwards, or *vice versa*. These surfaces are subaerial unconformities, transgressive ravinement surfaces, maximum regressive surfaces and maximum flooding surfaces (see Catuneanu et al., 2009). Aerial photographs and panoramic photomosaics of the outcrops were utilized for mapping, sequence stratigraphic analysis and correlation of sequences along the study area.

The geochemical analysis of $\delta^{13}C$ and $\delta^{18}O$ was measured on 66 bulk rock samples of limestones, marly limestones and marls, using standard analytical techniques. Samples were taken about every 2 m in the Barranco de las Calzadas (Forcall Formation) and were analyzed, using for each analysis 60-70 µg for limestones and 100-1000 µg for marls and marly limestones. Carbonate powder from limestones was extracted with a microdrill in order to avoid large skeletal components, corals, microencrusters and diagenetic calcite veins. The samples were treated with H_3PO_4 (100%) at 70 °C and the evolved CO_2 was analyzed with a Thermo Finnigan MAT-252 stable isotope ratio mass spectrometer in the *Unitat de Medi Ambient - Serveis Científicotècnics de la Universitat de Barcelona* laboratory. The isotope results are expressed in ‰ relative to the VPDB standard, and their precision was ± 0.03 for $\delta^{13}C$ and ± 0.06 for $\delta^{18}O$.

In order to explain the accommodation changes, quantitative subsidence analysis was carried out on five selected representative stratigraphic columns using standard back-stripping methods (Sclater and Christie, 1980; Watts,

1981; Bond and Kominz, 1984). Variables used in these techniques concerned lithology, absolute age (based on Ogg and Ogg, 2006) and palaeobathymetry values that were estimated from fossil assemblages and hydrodynamic structures. Density values for each type of lithology and porosity/depth relationships (c factors) were used to calculate decompaction (Sclater and Christie, 1980; Schmoker and Halley, 1982). No eustatic corrections were performed. The total subsidence (decompacted) was calculated for each selected stratigraphic section. The total accommodation was obtained from the total subsidence corrected with estimated palaeo-water depth values (Vilas et al., 2003).

FACIES EVOLUTION AND SEQUENCE STRATIGRAPHY

The Aptian sedimentary evolution and sequence stratigraphical framework of the Galve sub-basin is here presented in detail for the twelve studied outcrops. Ten facies assemblages ranging from continental to basinal were defined from lithology, texture, skeletal and non-skeletal components, sedimentary structures and the stratigraphic context. Each facies assemblage reflects a specific depositional environment based on inferred bathymetry and hydrodynamic conditions. The facies assemblages are described and classified in Table 1, and illustrated in Figs. 3, 4A-D and 4F. Moreover, four large-scale T-R sequences were interpreted based on the observed facies succession and the recognition of ten main surfaces with sequence stratigraphical implications. Together the sequences span the entire duration of the Aptian, about 13 Myr (according to the Aptian absolute ages from Ogg and Ogg, 2006). A chart displaying the distribution of the facies assemblages and sequence stratigraphy analysis for the five sections from the eastern side of the Miravete fault is shown in Fig. 5. The chart for the remaining seven sections on the western side is displayed in Fig. 6. A sequence stratigraphic interpretation of the exposure on the eastern side Las Cubetas section and the western side Villarroya de los Pinares section is shown in Fig. 7.

Sequence I

Sediments deposited during this sequence, which spans approximately 1 Ma (according to the Aptian absolute ages of Ogg and Ogg, 2006), mainly constitute the Morella and Xert formations (Fig. 2). The age of these deposits has been determined based on the identification of the magnetic anomaly M0r in the Morella Formation (Salas et al., 2005) and the recognition of the *Deshayesites weissi* biozone at the lower part of Sequence II (Moreno-Bedmar et al., 2009, accepted). Accordingly, these sediments could be correlatable with the *Deshayesites oglanlensis* biozone. Sequence I reaches a maximum thickness of up to 193 m in the Barranco de las Calzadas section, and thins to 38 m in the Cabezo de las Hoyas section.

Eastern side

The basal boundary of Sequence I is represented by a transgressive ravinement surface that separates the Barremian mixed carbonate-siliciclastic marine deposits (below) from the Aptian shallow-water carbonate and siliciclastic marine sediments of the Xert Formation (above). The transgressive systems tract (TST) of this sequence is distinguished by an initial wedge of high energy deposits stacked in a retrogradational pattern that thickens landwards. From the Cabezo de las Hoyas section to the south (basinwards), these high energy lithofacies grade into marls and limestones dominated by large-sized discoidal *Palorbitolina lenticularis*, which agglutinated quartz grains.

During the early transgressive phase, the eastern side tectonics probably positioned the Alto del Collado section area as a wave-influenced threshold zone. This circumstance isolated the area from direct detrital influx, favouring the deposition of peloidal-bioclastic grainstones containing skeletal fragments and benthic foraminifera such as miliolids, *Choffatella decipiens* and small-sized conical orbitolinids. The Alto del Collado palaeohigh evolved within the late TST to limestones rich in *Palorbitolina lenticularis*. In addition, episodes of sedimentation below fair-weather wave base during the TST are indicated by the intercalation of floatstones with miliolids, dasycladaceans (Fig. 3A), small requieniid rudists and *Chondrodonta* in the Cabezo de las Hoyas and Alto del Collado sections. According to Vennin and Aurell (2001) and due to the lack of bulging of sedimentary bodies or step-like geometries, the eastern side depositional profile corresponded to a homoclinal type of ramp (Fig. 5).

The transition between the TST and the regressive systems tract (RST) is marked by a facies change between the transgressive siliciclastic and orbitolinid-rich deposits, and the regressive carbonate lithologies dominated by dasycladaceans, miliolids, *Choffatella decipiens*, *Palorbitolina* sp., *Orbitolinopsis praesimplex* (Fig. 3B), unidentified benthic foraminifera, *Chondrodonta* and other molluscs. Interbedded sandy limestones and peloidal-bioclastic grainstones displaying cross-bedding and plane-parallel stratification also occur. These latter are mostly present along the middle-lower ramp, and signify the basinwards progradation during regression of the energetic facies trend formed in the upper ramp during the previous transgression (Fig. 5).

Western side

The lower boundary of the sequence corresponds to a subaerial unconformity, which separates Barremian carbonate and siliciclastic marine sediments (below) from the basal Aptian non-marine deposits of the Morella Formation (above). The Morella Formation consists of fluviatile sedi-

TABLE 1 | **Facies classification and interpretation of depositional environment.**

FACIES ASSEMBLAGE	DESCRIPTION	MAIN CONSTITUENTS	OTHER COMMON ELEMENTS	SEDIMENTARY FEATURES	DEPOSITIONAL ENVIRONMENT
1	Sandstones and red clay	Quartz, mica and feldspar	Dinosaur remains and fragments of wood	Low angle cross-bedding or plane-parallel stratification, and occasionally, massive or nodular bedding; tidal bundles (occasionally); crevasse splay structures (occasionally); basal lag deposits; root bioturbation (occasionally); erosive bases	Fluvial with tidal influence, low- to high-energy conditions. Supratidal to intertidal.
2	Ferruginous ooid grainstones, sandstones, sandy limestones and tan clay	Quartz, ooids and peloids	Mica, feldspar, oncoids, glauconite (occasionally), orbitolinids, miliolids, other foraminifera, oysters, unidentified bivalves, brachiopods (rarely) and fragments of gastropods, other molluscs, serpulids, bryozoans, echinoids, dasycladaceans and red algae	Low angle cross-bedding, plane-parallel or massive stratification, and occasionally, nodular bedding or herringbone stratification; unidentified burrows; *Lithophaga* borings (occasionally); hardgrounds; erosive bases	Marine shallow-water, low- to high-energy conditions. Intertidal to subtidal.
3	Sandstones, sandy limestones, ooid-peloid grainstones and bioclastic calcarenites	Quartz, mica, feldspar, ooids, peloids, miliolids, other foraminifera, and fragments of gastropods, echinoids and bivalves	Orbitolinids, oncoids, glauconite (occasionally), and fragments of corals, *Chondrodonta*, unidentified oysters, rudists, other molluscs, serpulids, bryozoans, red algae and dasycladaceans	Low angle cross-bedding, plane-parallel or massive stratification, and occasionally, herringbone stratification; tidal bundles (occasionally); tidal channels (occasionally); tidal bars (occasionally); unidentified burrows; hardgrounds; erosive bases	Marine shallow-water, moderate- to high-energy conditions. Intertidal to subtidal.
4	Mudstones and rudist-dominated wackestone to floatstone	Requieniid and elevator rudists, branching corals and miliolids	Sheet-like, platy and irregular massive corals, gastropods, *Chondrodonta*, oysters, unidentified bivalves, echinoids, orbitolinids, sessile foraminifera, other foraminifera, bryozoans, dasycladaceans, red algae, codiaceans and peloids (occasionally)	Massive or nodular bedding; *Lithophaga* borings; unidentified burrows (occasionally); hardgrounds (occasionally)	Below fair-weather wave base to below storm wave base, low-energy conditions. Subtidal.
5	Limestones bearing scattered massive corals	Irregular massive corals	Sheet-like, platy and domal corals, coral debris, orbitolinids, sessile foraminifera, other foraminifera, encrusting red algae, gastropods, bryozoans, echinoids, rudists, unidentified bivalves, *Lithocodium aggregatum*, *Bacinella irregularis* and peloids	Massive or nodular bedding; *Lithophaga* borings	Below fair-weather wave base to below storm wave base, low-energy conditions. Subtidal.
6	Dome-shaped corals embedded in marls	Domal corals	Sheet-like, branching and irregular massive corals, *Chondrodonta*, oysters, elevator rudists, unidentified bivalves, gastropods, echinoids, brachiopods and hydrozoans	*Lithophaga* borings; unidentified burrows (occasionally)	Below storm wave base, low-energy conditions. Subtidal.
7	Orbitolinid-dominated wackestone to grainstone	Orbitolinids	Peloids, sessile foraminifera, other foraminifera, oysters, unidentified bivalves, echinoids, gastropods, serpulids, bryozoans, belemnites, fish teeth, and fragments of undiagnosed molluscs, corals and dasycladaceans	Massive or nodular bedding, and occasionally, plane-parallel stratification; unidentified burrows and occasionally, *Thalassinoides*; hardgrounds (occasionally); erosive bases (occasionally)	Below fair-weather wave base to hemipelagic, low- to moderate-energy conditions. Subtidal.
8	Marls with interbedded storm-induced turbidites, marly limestones and mudstone to packstone limestones	Orbitolinids	Ammonites, nautiloids, oysters, unidentified bivalves, gastropods, echinoids, solitary corals, brachiopods, sessile foraminifera and occasionally, peloids, dasycladaceans, fish teeth, decapods, pyritized fragments and quartz	Massive or nodular bedding, and occasionally, plane-parallel stratification; *Thalassinoides* and other unidentified burrows; hardgrounds (occasionally); erosive bases (occasionally)	Hemipelagic, low- to moderate-energy, conditions. Subtidal.
9	Coral rubble encrusted by microorganisms	*Lithocodium aggregatum*, *Bacinella irregularis*, coral debris and orbitolinids	Encrusting red algae, sessile foraminifera, brachiopods, serpulids, briozoans, sponges, echinoids, corals, oysters, caprinid rudists and solitary corals	Nodular bedding	Below fair-weather wave base to hemipelagic, low- to moderate-energy conditions. Subtidal.
10	Rudist-dominated wackestone to rudstone debris flows	Requieniid and elevator rudists, miliolids and fragments of corals and rudists	Peloids, orbitolinids, other foraminifera, *Lithocodium aggregatum*, *Bacinella irregularis*, and fragments of gastropods, bryozoans, *Chondrodonta*, oysters, unidentified bivalves, other molluscs, echinoids, encrusting red algae, dasycladaceans and codiaceans	Massive or nodular bedding; unidentified burrows; slump scars (occasionally); erosive bases	Below fair-weather wave base to hemipelagic, low- to moderate-energy conditions. Subtidal.

ments made up of red clay and channelized sandstones (Fig. 4A), occasionally reworked by tidal currents, which become progressively more marine in character upwards in the succession. This formation is only recorded on the western side of the Miravete fault (Fig. 6). During the earliest Aptian, the Miravete fault apparently acted as a trap for these continental deposits, and retained them in the hanging-wall block. The Morella Formation changes laterally to the marine siliciclastic-influenced sediments of the Xert Formation. The TST exhibits greater thicknesses and reflects deeper environments than in the east side. The siliciclastic wedge is made of fining-upwards tidal channel and bar deposits displaying erosive bases, tidal bundles, cross-bedding and herringbone cross-stratification. Bioturbation is commonly present, as well as oysters, unidentified bivalves and the infaunal echinoid *Heteraster oblongus*. Basinwards, these deposits are interbedded with marls rich in mica. The intertidal lithofacies evolve upwards and laterally to marls and limestones with abundant large-sized discoidal *Palorbitolina lenticularis*, which agglutinated minute quartz grains. At the distal Barranco del Portolés and Villarroya de los Pinares sections, especially in their uppermost TST, these orbitolinid-rich carbonates alternate with oolitic-bioclastic packstones to grainstones containing miliolids, *Choffatella decipiens*, other unidentified foraminifera and skeletal fragments (Fig. 6).

The maximum flooding surface is marked by a facies turnover from transgressive *Palorbitolina*-dominated beds to regressive wackestone to floatstone limestones containing *Chondrodonta*, small requieniid rudists, other molluscs, miliolids, *Choffatella decipiens*, *Palorbitolina praecursor*, *Orbitolinopsis* sp., *Rectodictyoconus giganteus* and other benthic foraminifera. Locally, bioturbated horizons occur. The lateral continuity of beds that thicken in a southerly direction together with the absence of bulges or step-like geometries indicate that the depositional profile during the RST was a homoclinal carbonate ramp, as inferred on the eastern side for the same time interval (Fig. 6).

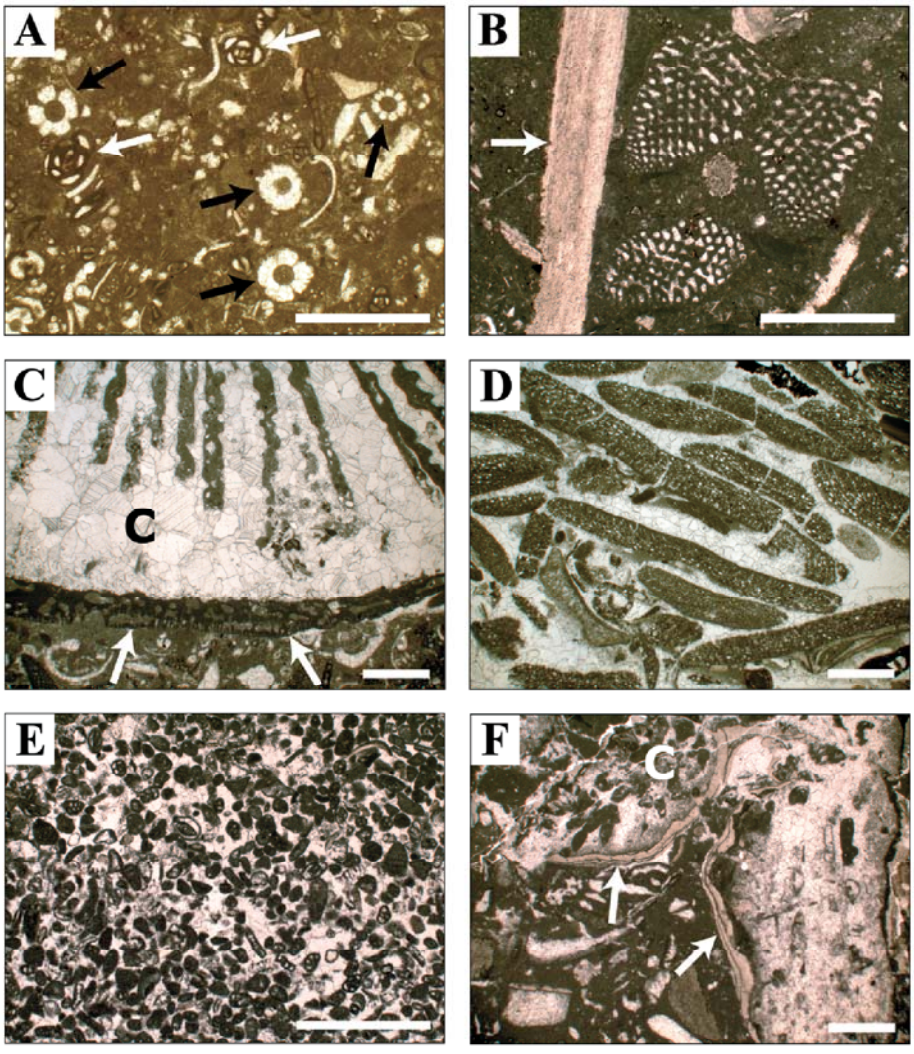

FIGURE 3 | **Photomicrographs of representative microfacies of the different general depositional settings. Scale bars = 1mm. A) Wackestone of miliolids (white arrows) and fragments of dasycladaceans (black arrows) (Facies Assemblage 4; Table 1). Xert Formation, Alto del Collado section. B) Floatstone of *Chondrodonta* with *Orbitolinopsis praesimplex*. The white arrow points to a fragment of *Chondrodonta* (Facies Assemblage 4; Table 1). Xert Formation, Las Cubetas section. C) *Lithocodium aggregatum* (white arrows) bioeroded by clionid sponges, encrusting coral debris (black C) (Facies Assemblage 9; Table 1). Forcall Formation, Estrecho de la Calzada Vieja section. D) Grainstone of large-sized discoidal *Palorbitolina lenticularis* agglutinating quartz particles in the tests (Facies Assemblage 7; Table 1). Villarroya de los Pinares Formation, Las Cubetas section. E) Peloidal-foraminiferal (mostly miliolids) grainstone (Facies Assemblage 3; Table 1). Villarroya de los Pinares Formation, Barranco de las Calzadas section. F) Debris-flow facies of coral fragments (white C) and other unidentified bioclasts encrusted by peyssonneliaceans (white arrows) (Facies Assemblage 10; Table 1). Villarroya de los Pinares Formation, Barranco de las Calzadas section.**

Sequence II

Sequence II is equivalent to the Forcall and the main part of the Villarroya de los Pinares formations (Fig. 2). On the western side, the top of the Xert Formation also belongs to the basal transgressive deposits of this sequence, which spans approximately 3 Ma (according to the absolute ages for the Aptian of Ogg and Ogg, 2006), and reaches its maximum thickness of up to 237 m in the Barranco de las Calzadas section. At the Alto del Collado section the sequence thins to 141 m. The recognition of the ammonite species *Deshayesites kiliani* at the lower part of this sequence permits us to constrain its base to the *Deshayesites weissi* biozone. The lower boundary of the sequence is formed by a sharp contact, which corresponds to a maximum regressive surface, though no signs of subaerial exposure or erosion were identified. This sequence boundary is marked by a drastic facies change, which separates the carbonate lithologies with small requieniid rudists, miliolids and *Chondrodonta* of the uppermost part of the Xert Formation (below) from the transgressive green marls of the Forcall Formation (above). On the western side, these basal transgressive deposits correspond to orbitolinid-dominated beds, which constitute the top of the Xert Formation. With the early TST, the incipient carbonate platforms established during the regressive phase of Sequence I were drowned and evolved into a succession of interbedded green marls, marly limestones, silty limestones and limestones displaying frequent nodular bedding and burrow bioturbation. Its faunal content suggests deeper water conditions and is characterized by the bivalves *Panopea* sp., *Trigonia* sp. and *Neithea* sp., other molluscs, the echinoid *Heteraster oblongus*, terebratulid brachiopods, *Palorbitolina lenticularis*, *Praeorbitolina cormyi*, *Palorbitolina* sp., *Choffatella decipiens* and other undiagnosed foraminifera. The orbitolinids present large-sized discoidal morphologies and agglutinated quartz grains. At the proximal sections of Camarillas and Loma del Horcajo it is

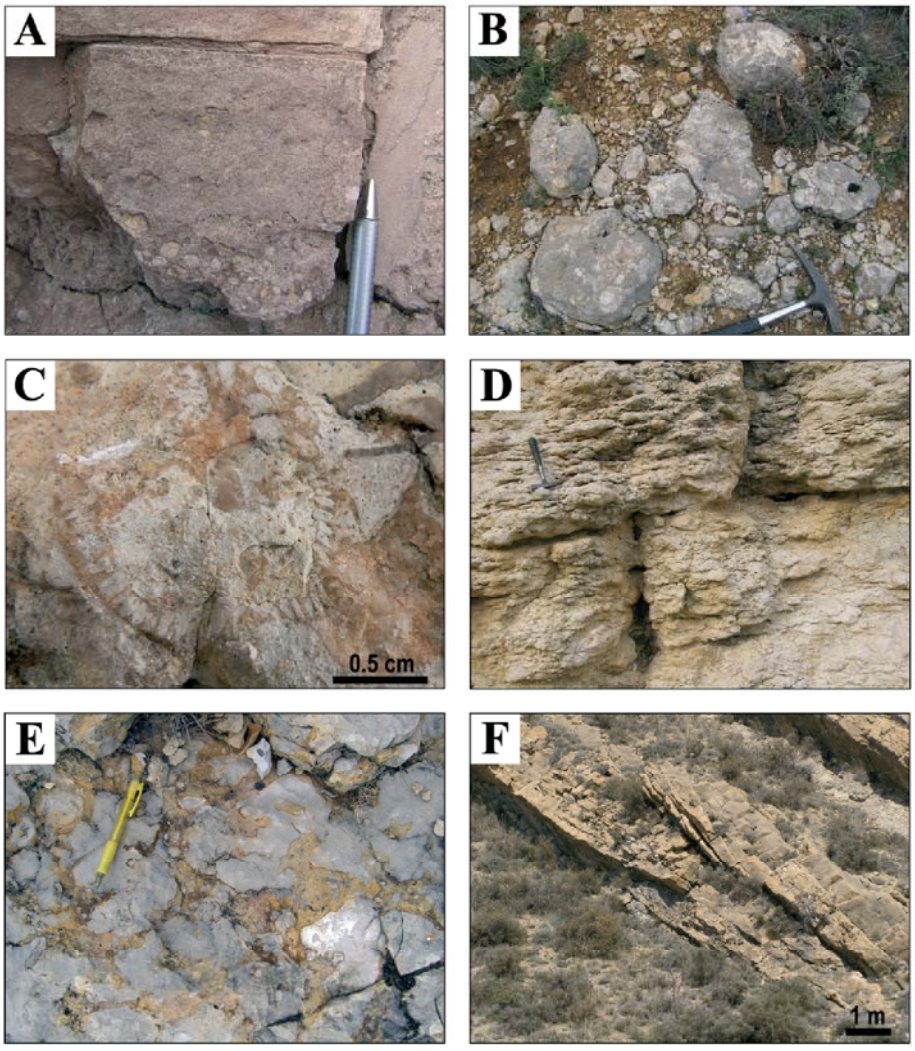

FIGURE 4 | **Outcrop photographs of representative facies of the general depositional settings. A) Detail of a coarse-grained siliciclastic lag at the erosive base of a channelized sandstone (Facies Assemblage 1; Table 1). Morella Formation, Barranco de las Calzadas section. B) Dome-shaped corals embedded in marls (Facies Assemblage 6; Table 1). Villarroya de los Pinares Formation, Barranco de las Calzadas section. C) Detail of a *Caprina parvula* section (Facies Assemblage 4; Table 1). Villarroya de los Pinares Formation, Barranco de las Calzadas section. D) Outcrop-scale image of debris-flow deposits (Facies Assemblage 10; Table 1). Note the nodular aspect of these resedimented lithofacies. Villarroya de los Pinares Formation, Barranco de las Calzadas section. E) Detail of the boundary surface between Sequence II and Sequence III exhibiting palaeokarst development. Villarroya de los Pinares Formation, Camarillas section. F) Detail of a herringbone cross-stratification (Facies Assemblage 2; Table 1). Benassal Formation, Barranco del Portolés section.**

common to find intercalations of sandy limestones, peloidal grainstones displaying plane-parallel stratification and layers with abundant green algae and molluscs, denoting shallower environments (Figs. 5 and 6).

An orbitolinid-dominated stratigraphic interval, composed of nodular bioturbated limestones showing a more carbonate-rich lithology, interrupts these marly-dominated deposits. The episode is continuous and correlatable along the sub-basin except in the Loma del Horcajo and Camarillas sections, where it was not identified, probably due to their proximal setting. Above this, another flooding pulse occurs, with recovery of the marly condition of elsewhere in the succession. At the western side, this deepening is made more evident by the occurrence of a few levels with *Heminautilus saxbii* and ammonites belonging to the *Roloboceras hambrovi* horizon (Moreno-Bedmar et al., 2009). The late TST is characterized by several layers containing abundant orbitolinids at the base of coral rubble deposits, up to 5 m thick, which are completely encrusted by *Lithocodium aggregatum* (Fig. 3C), *Bacinella irregularis* and sessile foraminifera. Abundant *Palorbitolina lenticularis* displaying large discoidal morphologies and agglutinating quartz particles, echinoids, solitary corals, the rudists *Caprina douvillei* and *Horiopleura dumortieri* are also found inside the *Lithocodium*/*Bacinella*-coral rubble horizon. The maximum flooding surface is interpreted to underlie the coral rubble deposits, which therefore constitute the earliest RST (Figs. 5 and 6).

Eastern side

The early RST begins with several microorganism-encrusted coral rubble layers, which change laterally southwards and upwards in the succession to interbedded marls and limestones with abundant large-sized discoidal *Palorbitolina lenticularis* with agglutinated quartz particles. At the Alto del Collado section, a specimen of *Deshayesites deshayesi* was recognized, establishing the presence of the *Deshayesites deshayesi* biozone above the *Lithocodium*-coral rubble horizon. Above the latter, widespread *Palorbitolina lenticularis* beds mark the beginning of the Villarroya de los Pinares Formation and are followed by limestones with sparsely distributed irregular massive corals. The coral-bearing limestones, which reach up to 15 m thick in the Cabezo de las Hoyas section, form a continuous level from the Loma del Horcajo section to the Estrecho de la Calzada Vieja section, and pinch out into marls after this last-mentioned section. Fragments of molluscs, abundant *Palorbitolina lenticularis*, *Praeorbitolina cormyi*, other unidentified foraminifera, and *Lithocodium aggregatum*, *Bacinella irregularis* and sessile foraminifera encrusting the corals, are also important components of the facies. However, the abundance of microencrusters is not as significant as for the preceding coral rubble episodes. Above this, the RST exhibits a progradational pattern of sedimentary bodies grouped in metre-thick small-scale sequences. This part of the succession is distinguished by the development of abundant carbonate producers such as *Toucasia carinata*, *Polyconites* new species (Skelton et al., in press) grouped in bouquets, small specimens of an unidentified monopleurid, *Chondrodonta*, other molluscs, corals, miliolids, *Orbitolinopsis simplex*, *Orbitolinopsis praesimplex* and other unidentified foraminifera. Burrow bioturbation and hardgrounds with encrusting oysters are also common (Fig. 5).

The depositional profile during this regressive stage corresponded to a distally steepened ramp with most carbonate production situated in the upper ramp. Where synsedimentary normal faulting caused major steepening of the ramp approximately south of the Cabezo de las Hoyas section (Fig. 8), the latter lithofacies pass basinwards to debris-flow deposits. Marls with embedded dome-shaped corals displaying *Lithophaga* borings are intercalated between these resedimented lithofacies. In addition, a synsedimentary fault located southwards of the Estrecho de la Calzada Vieja caused a second steepening of the ramp as deduced by the bulging and step-like geometries of the beds (Fig. 8). Distal ramp facies were recognized in the Alto del Collado section, which correspond to eight high-order cycles composed of centimetric mudstones overlain by decimetric floatstones containing fragments of *Chondrodonta*, rudists and delicate branching corals. The mudstones are interpreted to reflect parautochthonous sedimentation, while the floatstones, in which all skeletal components are fragmented, correspond to debris-flow episodes. In the Las Cubetas section, a facies representing a short episode of platform crisis has been found intercalated between limestones dominated by miliolids, corals, rudists and other molluscs. This episode is distinguished by two units of rock-forming *Palorbitolina lenticularis* and a 1.5 metre-thick level of coral rubble encrusted by *Lithocodium aggregatum*, *Bacinella irregularis* and sessile foraminifera. The presence of coral rubble and orbitolinid beds displaying packstone to grainstone textures indicates reworking. The orbitolinids exhibit large flat morphologies with abundant quartz aggregation (Fig. 3D) (Fig. 5).

Western side

Above the encrusted coral rubble deposits, the RST reveals the bathymetric differences between the eastern side (foot-wall) and the western side (hanging-wall) of the Miravete fault. The sedimentary record exhibits larger thicknesses and is built-up of small-scale sequences (in the sense of Strasser et al., 1999) each with a centimetre- to metre-thick marly transgressive term, and a centimetre- to decimetre-thick regressive term, comprising marly limestones, sandy/silty limestones and/or limestones displaying

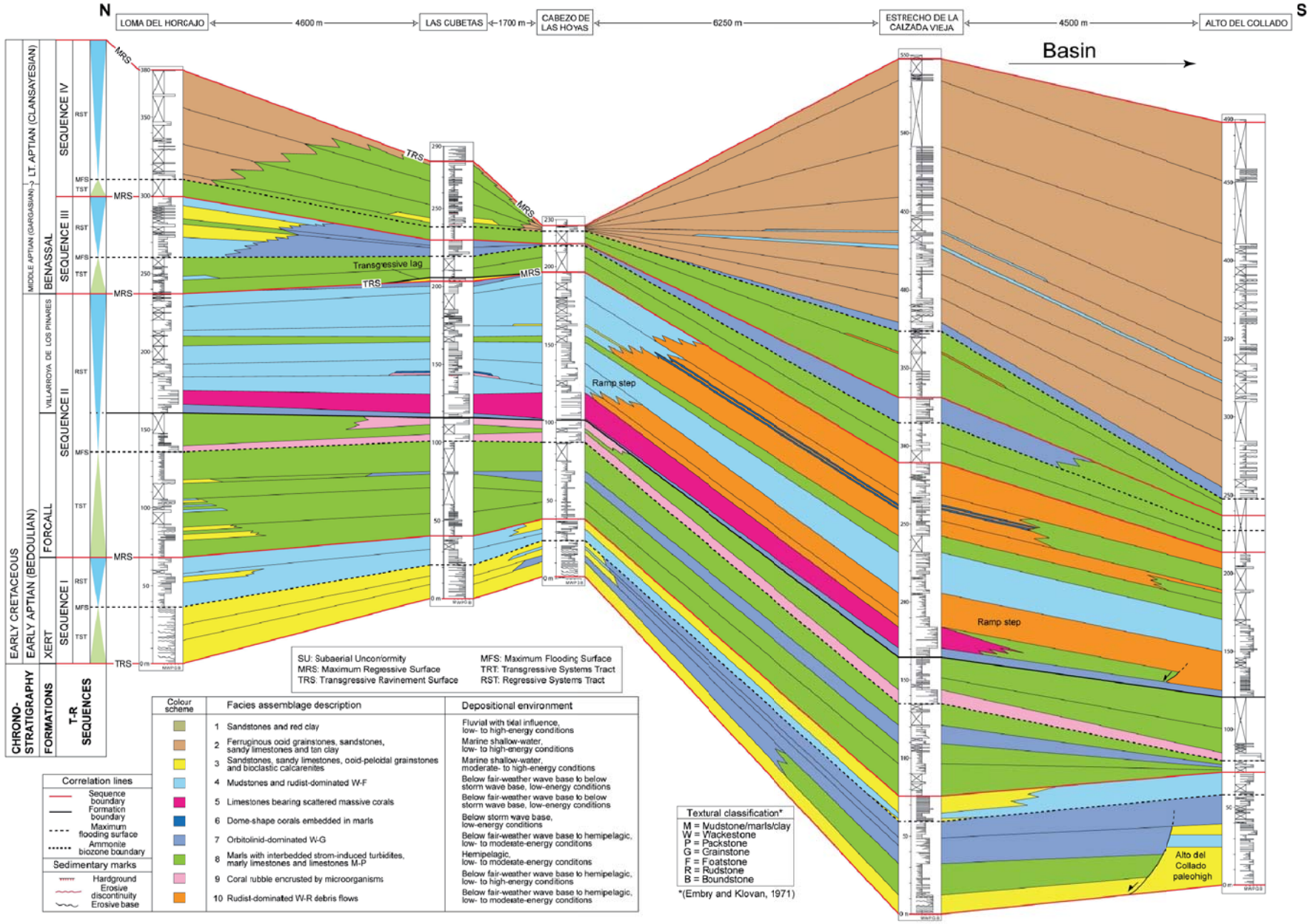

FIGURE 5 | **Eastern side sequence correlation scheme and distribution of the facies assemblages.**

T. BOVER-ARNAL et al. The Aptian evolution of the western Maestrat Basin

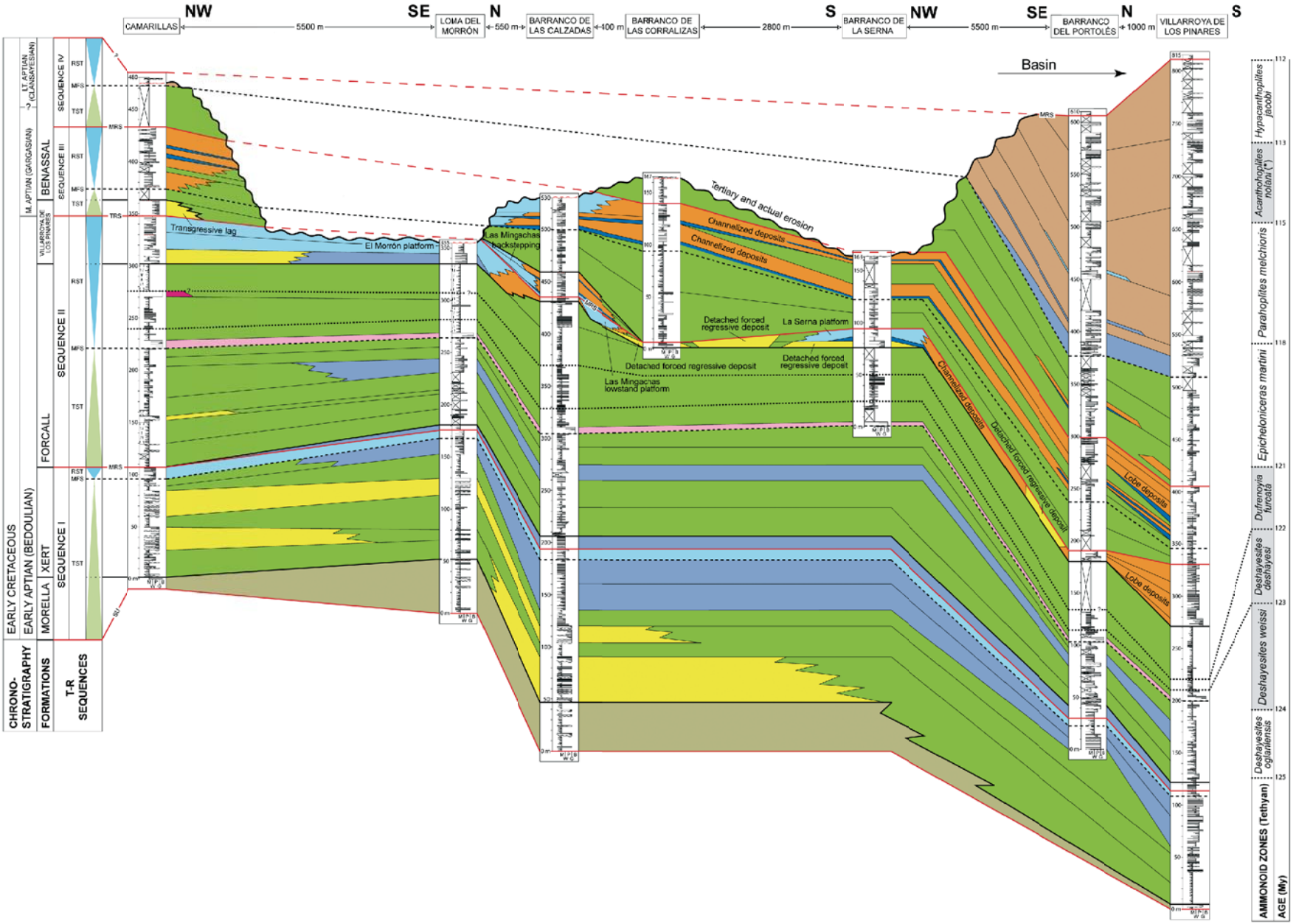

FIGURE 61 | **Western side sequence correlation scheme and distribution of the facies assemblages. Identified ammonite biozones are indicated in grey. See Fig. 5 for legend.**

T. BOVER-ARNAL et al. The Aptian evolution of the western Maestrat Basin

nodular bedding. *Thalassinoides* and other burrow bioturbation are common, especially at the bases of the regressive layers and local levels with storm-induced turbidites (see Bover-Arnal et al., 2009). The faunal content also reflects a deeper environment than in the eastern part of the sub-basin, and is characterized by ammonites, terebratulid and rhynchonellid brachiopods, solitary corals, the orbitolinids *Palorbitolina lenticularis* and *Praeorbitolina gr. cormyi-wienandsi*, which commonly agglutinated quartz particles and exhibit large-sized discoidal morphologies. Also present are the nautiloids *Eucymatoceras plicatum* and *Cymatoceras neckerianum*, the bivalves *Trigonia* sp., *Plicatula placunea*, *Panopea* sp. and *Neithea* sp., other unidentified molluscs, the echinoid *Toxaster collegnoi* and the decapod *Mecochirus magnus*. Pyritized fragments also occur. A 5-metre level of centimetre-sized coral colonies is present in the proximal section of Camarillas. The ammonite record, which is abundant and complete, especially in the Barranco de las Calzadas section (Moreno-Bedmar et al., 2009, accepted) provided two timelines for the Bedoulian (Early Aptian): the *Deshayesites weissi* biozone-*Deshayesites deshayesi* biozone boundary, and the *Deshayesites deshayesi* biozone-*Dufrenoyia furcata* biozone boundary (Fig. 6).

Above this, the regressive succession corresponds to the lower part of the Villarroya de los Pinares Formation, and is distinguished by below-wave base accumulation of carbonate-producing biota dominated by the rudists *Toucasia cari-*

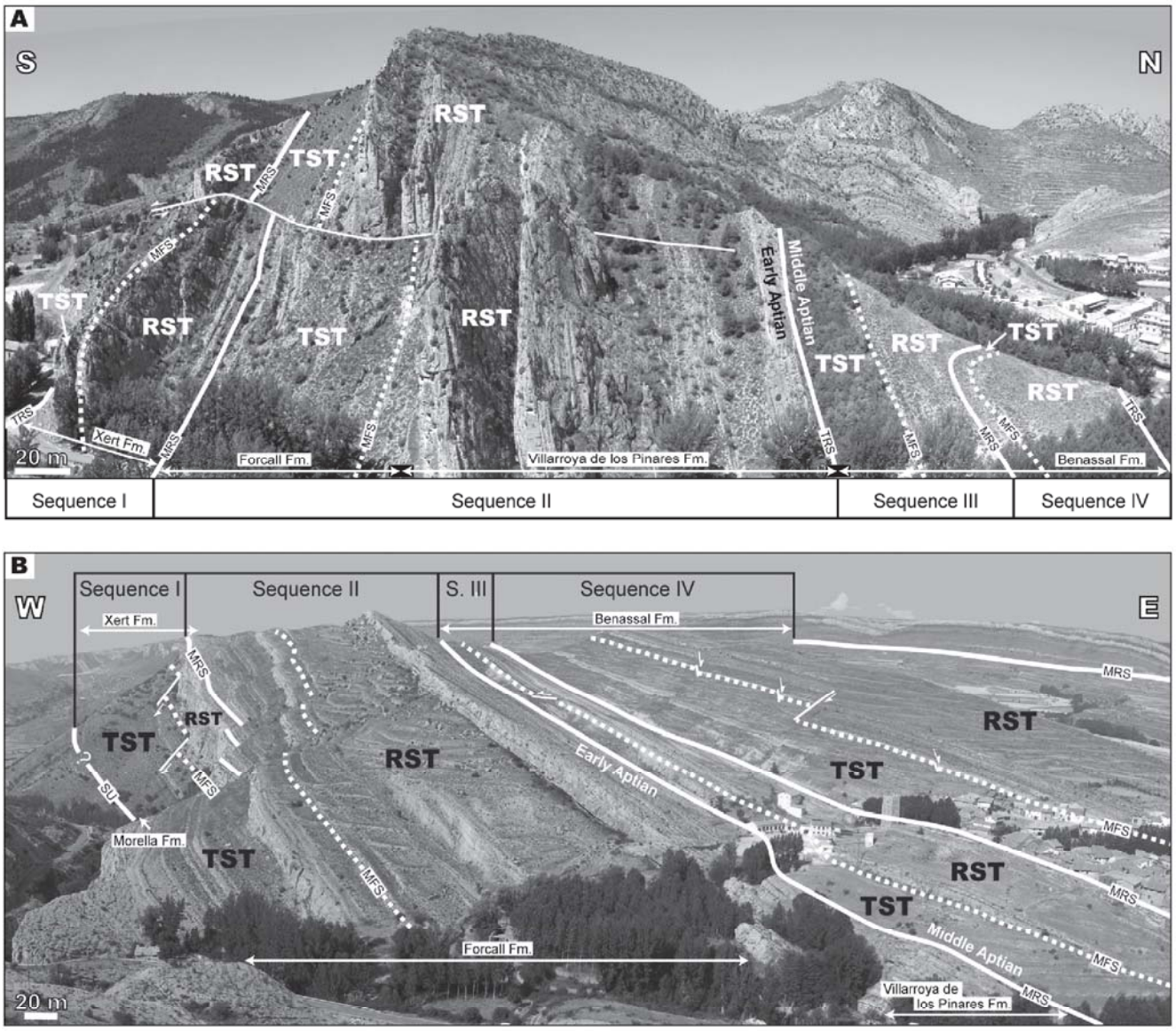

FIGURE 7 | **Sequence stratigraphic interpretation of A) the Aptian sedimentary succession in the Las Cubetas section (eastern side of the Miravete fault) and B) the Villarroya de los Pinares section (western side of the Miravete fault). See Fig. 5 for legend.**

nata and *Polyconites* new species (Skelton et al., in press), with rarer *Monopleura* sp., *Caprina parvula* (Fig. 4C) and *Offneria* sp. Also present are *Chondrodonta*, nerineid gastropods, other undiagnosed molluscs, corals, *Orbitolinopsis simplex*, miliolids, other benthic foraminifera and green algae. Intercalation of plane-parallel stratified oolitic-peloidal grainstones with abundant miliolids and other unidentified benthic foraminifera also occur (Fig. 3E), indicating short higher energy episodes. The sedimentary bodies are stacked in a prograding pattern constituting metre-thick small-scale sequences. In the Camarillas and the Barranco de la Serna sections, this late RST starts with fine-grained sandy limestones and calcarenites displaying cross-bedding and plane-parallel stratification. The depositional profile corresponds to a flat-topped non-rimmed carbonate platform (see Bover-Arnal et al., 2009), which is continuous from the Camarillas section to the Loma del Morrón section, where the platform margin is situated. Basinwards, these platform facies change laterally into debris-flow deposits (Fig. 3F), which are locally channelized, and marls with embedded dome-shaped corals (Fig. 4B), representing the slope environments. Irregular massive, sheet-like and branching corals, and *Polyconites* grouped in bouquets are also present in this depositional setting (Fig. 6).

In the Barranco de la Serna section, the carbonate platform established during this time interval shows detached development due to its palaeosituation in an upthrown part of a half-graben structure related to the ENE-WSW normal listric faulting (Fig. 1B). This isolated platform is characterized by the presence of large delicate branching corals, *Toucasia carinata* and caprinid rudists, including *Caprina parvula* and *Pachytraga* sp. Southeastwards, it passes laterally to slope lithofacies. In the Barranco del Portolés and Villarroya de

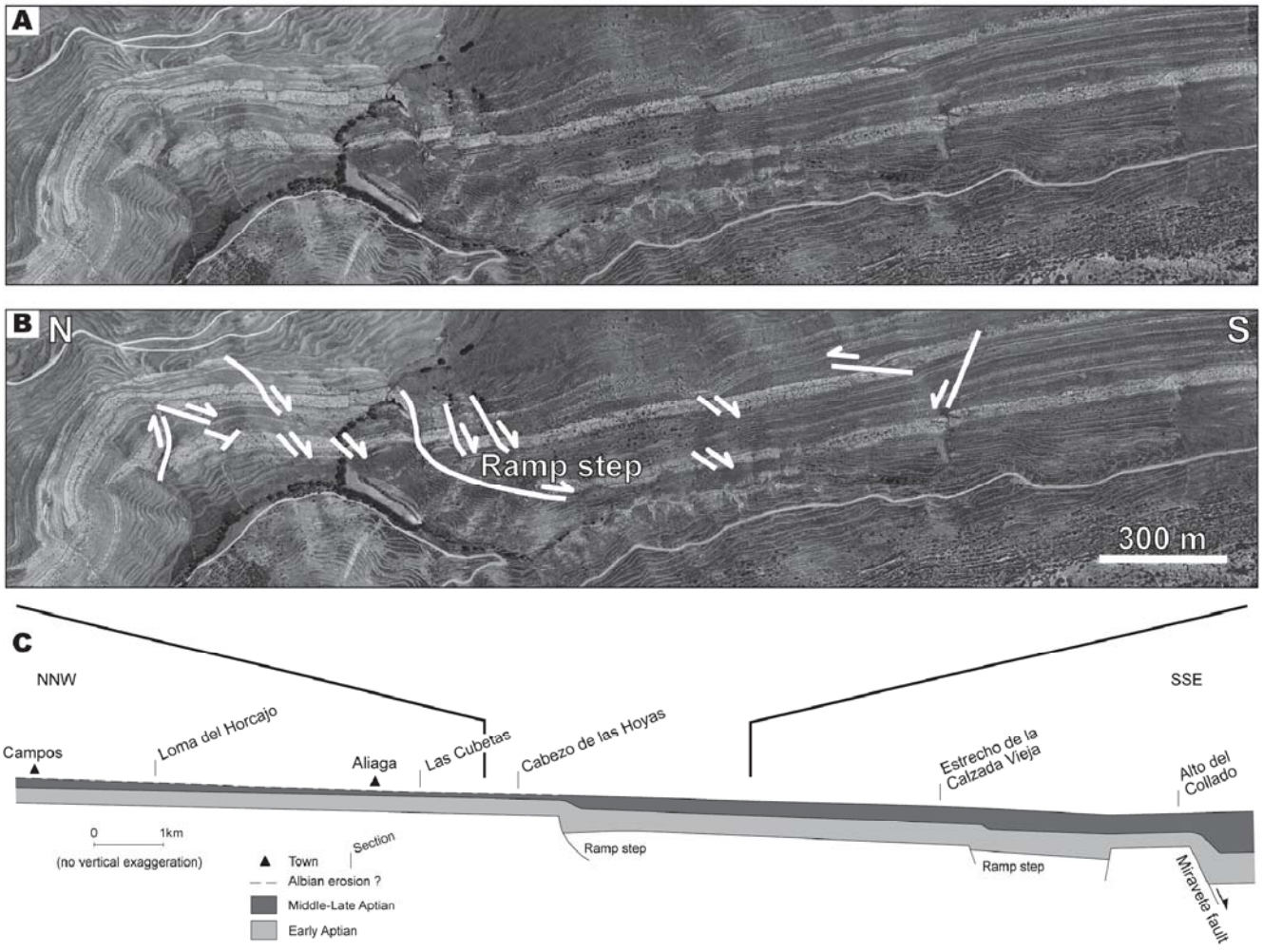

FIGURE 8 | **A) Aerial photograph of the area surrounding the Cabezo de las Hoyas section (see Fig. 1B for location), which belongs to the eastern side of the Miravete fault. B) Interpreted aerial photograph with the situation of the major ramp step located southwards of the Cabezo de las Hoyas section. C) Schematic cross-section of the eastern side distally steepened ramp of Sequence II showing the situation of the two steps located nearby to the south of the Cabezo de las Hoyas section and southwards of the Estrecho de la Calzada Vieja section. The depositional profile was reconstructed from the aerial photo. See Fig. 1B for situation.**

los Pinares sections, the late regressive phase corresponds to basinal debris-flow deposits accumulated in lobes. In the Barranco de las Calzadas section, the sediments that mark the top of the RST of Sequence II constitute a lowstand prograding wedge in the sense of Hunt and Tucker (1992). This lowstand wedge corresponds to a small prograding flat-topped non-rimmed carbonate platform situated in the area of Las Mingachas (see Bover-Arnal et al., 2009). Towards the basin, this lowstand carbonate platform changes laterally into slope lithofacies of debris-flows deposits (Fig. 4D) and marls with embedded dome-shaped, irregular massive and branching corals, which downlap over a detached forced regressive calcarenite situated in a basinal position. Basinwards, the maximum fall in sea level at the top of the RST is marked by several discontinuous cross-bedded and plane-parallel stratified calcarenites embedded in marls, which contain oysters, *Orbitolinopsis simplex*, *Palorbitolina lenticularis*, unidentified benthic foraminifera and fragments of molluscs, echinoids and decapods. These calcarenites constitute detached forced regressive deposits (Fig. 6).

Sequence III

Sequence III contains the lower part of the Benassal Formation (Fig. 2). In the Camarillas, Barranco de las Calzadas and Las Cubetas sections, Sequence III is also equivalent to the uppermost part of the Villarroya de los Pinares Formation. This sequence is interpreted to span approximately 3.1 Ma (according to the absolute Aptian ages of Ogg and Ogg, 2006), and has a maximum thickness of 135 m in the Barranco de las Corralizas section. In the Cabezo de las Hoyas section, this sequence thins to 20 m. Its base is early Middle Aptian in age, inferred from rudist biostratigraphy. The boundary between the sequences II and III appears to correspond to the limit between the Early (Bedoulian) and the Middle Aptian (Gargasian), where the rudist family Caprinidae disappears from all sections known so far (Skelton, 2003a).

Eastern side

In the Las Cubetas section an erosive surface has been identified at the top of the regressive deposits of Sequence II. This surface is interpreted as the sequence boundary between Sequence II and III and corresponds to a transgressive ravinement surface (Fig. 5). The unconformity is overlain by oolitic-peloidal grainstones with fragments of dasycladaceans and echinoids, which are interpreted to represent the transgressive lag of the TST of Sequence III. A hardground with encrusting oysters and borings marks the top of these hydrodynamic deposits. In the other sections studied on the eastern side of the Miravete fault, no signs of subaerial exposure or erosion have been identified above the prograding regressive deposits of Sequence II. Hence, the lower boundary of Sequence III is interpreted to be a maximum regressive surface. The TST of this sequence is characterized by marls with calcareous nodules. Upwards in the succession the presence of nodular limestones with large flat orbitolinids becomes dominant. The maximum flooding surface separates these marly facies from widespread limestones dominated by *Mesorbitolina parva* and *Mesorbitolina* gr. *lotzei-parva* that correspond to the RST and reflect a shallowing-upwards trend. Interbedded marls with calcareous nodules and peloidal-bioclastic grainstones are present, as well as highly bioturbated levels. In the Loma del Horcajo section, this orbitolinid horizon changes landwards to an alternation of limestones with rudists, coral fragments, nerineid gastropods, orbitolinids and miliolids, and sandstones and sandy limestones with cross-bedding and plane-parallel stratification, indicating a shallower and proximal setting with episodes of detrital influx (Fig. 5).

Western side

The basal boundary of the sequence records a relative sea level fall with subaerial exposure and erosion of the previous carbonate platform established during the late Early Aptian between the Camarillas and Loma del Morrón sections (Fig. 6). This discontinuity corresponds to a transgressive ravinement surface (Fig. 9) with palaeokarst features (Fig. 4E). Southwards of the Camarillas section, this sequence boundary is eroded, but it is interpreted as having continued until the Barranco de las Calzadas section, where it has also been identified. After this last-mentioned section and towards the basin, the transgressive ravinement surface changes to a maximum regressive surface. In the Camarillas section, the TST begins with a cross-bedded and plane-parallel stratified orange calcarenite containing oysters, foraminifera and fragments of echinoids and unidentified molluscs. This calcarenite is stacked in a retrograding pattern and represents the transgressive lag that onlaps the sequence boundary (Fig. 9). The base of this deposit is erosive and presents mud pebbles with minute imbricated quartz particles. A little way to the south of the Barranco de las Calzadas section, the onset of the TST is marked by a maximum regressive surface that corresponds to a hardground with a ferruginous crust and borings. This transgressive surface is situated above the lowstand prograding wedge established during the RST of Sequence II. Over the hardground, the lowstand prograding carbonate platform of Las Mingachas starts to backstep northwards (see Bover-Arnal et al., 2009), forcing the establishment of the typical slope facies association in this area. These lithofacies are distinguished by the settlement of domal, irregular massive and branching coral colonies embedded in marls, cut across by channelized debris-flow deposits. Above this and towards the basin, the transgressive phase changes laterally to bluish marly deposits with interbedded

calcareous nodules and nodular limestones containing *Mesorbitolina parva*, decapods, the nautiloid *Eucymatoceras plicatum*, echinoids, *Panopea* sp., *Trochonerita gigas*, *Tylostoma* sp. and other molluscs. Highly bioturbated levels are common. In the Barranco de las Corralizas section, there are interbedded sandy limestones displaying plane-parallel stratification (Fig. 6).

The maximum flooding surface marks a drastic facies change from marly sedimentation to below-wave base carbonate-platform production that characterizes the RST. However, this regressive stage mainly reflects sedimentation in slope environments. The slope lithofacies are characterized by small patch-reefs with domal, irregular massive and branching corals embedded in marls, *Polyconites* new species (Skelton et al., in press) grouped in bouquets, gastropods, oysters and other unidentified molluscs. Channelized debris-flow deposits of platform sediments with *Toucasia carinata* and nerineid gastropods cut across these marly deposits. In the Barranco del Portolés and Villarroya de los Pinares sections the debris-flow deposits are accumulated in lobes interbedded with marly levels containing calcareous nodules. Bioturbated levels are present throughout the regressive tract (Fig. 6).

Sequence IV

Sequence IV corresponds to the upper part of the Benassal Formation. It is interpreted to span approximately 5.9 Ma (according to the Aptian absolute ages from Ogg and Ogg, 2006), and comprises the upper part of the Middle Aptian (Gargasian) and the entire Late Aptian (Clansayesian) (Fig. 2). The age of the base of the sequence has not been exactly determined due to the absence of age-diagnostic fauna. Nevertheless, Weisser (1959) recognized an ammonoid specimen of *Acanthohoplites bergeroni*, which according to Bogdanova and Tovbina (1994) is attributable to the *Diadochoceras nodoscostatum* subzone (*Acanthohoplites nolani* biozone), in the basal regressive stage of this sequence. Moreover, Moreno-Bedmar et al. (2008) collected ammonite specimens from the *Leymeriella tardefurcata* biozone (basal Albian) in the lower part of the Es-

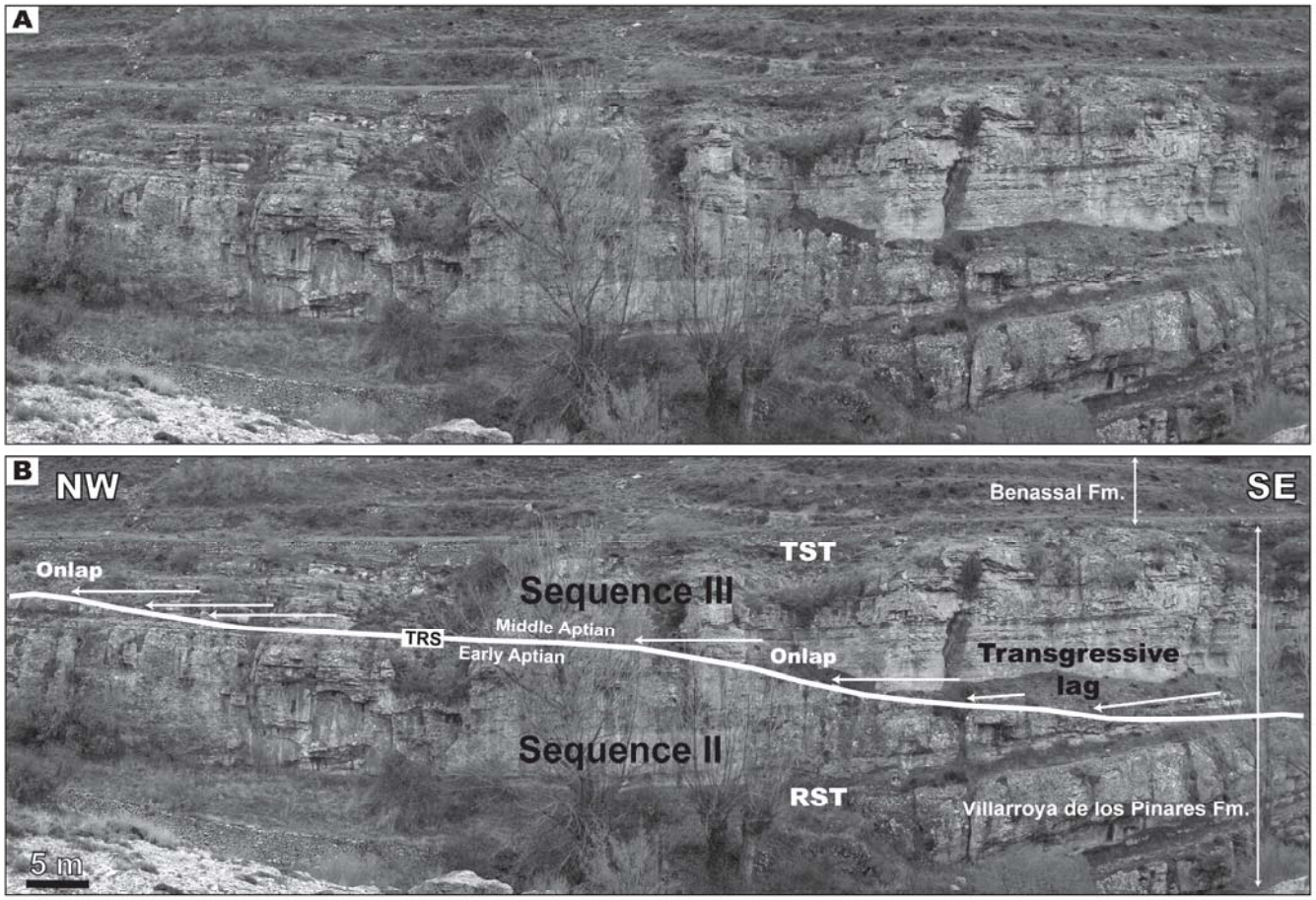

FIGURE 9 | **A) Outcrop-scale view of the boundary between Sequence II (Early Aptian) and Sequence III (Middle Aptian) located southwards of the Camarillas section (western side of the Miravete fault). B) Photograph interpretation of the boundary between Sequence II (Early Aptian) and Sequence III (Middle Aptian) located southwards of the Camarillas section (western side of the Miravete fault). See Fig. 5 for legend.**

cucha Formation, which overlies the Benassal Formation, in the Salzadella sub-basin nearby to the East. Villanueva-Amadoz et al. (2008) also determined an Early-Middle Albian age for the Escucha Formation using palynomorphs. The limit between the Benassal and Escucha formations is also equivalent to the upper boundary of Sequence IV. The upper limit of this sequence may thus be constrained effectively to the boundary between the Aptian and the Albian. The sequence has a maximum thickness of 410 m in the Villarroya de los Pinares section, and thins to 18 m in the Cabezo de las Hoyas section. The boundary between sequences III and IV corresponds to a maximum regressive surface, which has been recognized on both sides of the Miravete fault. This boundary is characterized by a drastic facies change from limestones deposited below wave influence, containing rudists, corals and orbitolinids, to marly sedimentation. At Las Cubetas this lower sequence boundary consists of a well-developed hardground. The upper sequence boundary is constituted by a regional unconformity, which passes basinwards to a maximum regressive surface, overlain by the white sandstones and coal deposits of the Escucha Formation.

Eastern side

The TST is represented by an alternation of marls with calcareous nodules and marly limestones containing *Mesorbitolina parva*, echinoids and molluscs. Occasionally, resedimented deposits of rudists and coral fragments with floatstone to rudstone texture occur. The maximum flooding surface marks a drastic change in the facies trend, from deepening to shallowing-upwards. The base of the RST is constituted by highly bioturbated orbitolinid beds with molluscs and echinoids. The presence of hardgrounds with encrusting oysters is common. Above this, an alternation of tan clay, oolitic-peloidal packstone to grainstone limestones, sandy limestones and sandstones with erosive bases, cross-bedding and plane-parallel stratification become dominant. Intercalation of two small layers with *Eoradiolites* sp., *Toucasia* sp. and small delicate branching corals has been observed in the distal parts of both eastern and western sides, indicating the establishment of two incipient carbonate platforms, which were soon suppressed, however, by the high current activity and detrital influx that prevailed during the regressive phase of Sequence IV (Fig. 5).

Western side

The TST is distinguished by bluish marls with calcareous nodules and marly limestones with nodular bedding, containing *Mesorbitolina parva*, oysters, unidentified bivalves, echinoids and gastropods. Intercalation of bioclastic-peloidal packstone to grainstone limestones with plane-parallel stratification, orbitolinid beds and sandy limestones indicate intermittent higher energy conditions or reworking. Pervasively bioturbated levels are common. Debris-flow deposits with floatstone to rudstone texture, containing rudists, orbitolinids, oysters and fragments of delicate branching corals are also present. Below these resedimented lithofacies dome-shaped and irregular massive corals are frequently found embedded in marls, which may represent slope environments. The maximum flooding surface is marked by an abrupt facies change, from a deepening to a shallowing-upwards trend. The RST begins with resedimented packstone to grainstone limestones of *Mesorbitolina parva* with erosive bases in the Barranco del Portolés and Villarroya de los Pinares sections. Above these orbitolinid beds, the establishment of littoral conditions is reflected by red oolitic-bioclastic grainstones with glauconite, sandy limestones, sandstones and tan clay. The beds feature erosive bases, cross-bedding, plane-parallel, herringbone stratification (Fig. 4F) and are occasionally channelized. Bioturbated levels, and hardgrounds with encrusting oysters and *Lithophaga* occur. The presence of mica is noticeable in the late regressive phase. Oysters, unidentified bivalves, echinoids, gastropods and rarely, brachiopods, dominate the faunal content (Fig. 6).

STABLE ISOTOPE (C, O) GEOCHEMISTRY

Carbonate carbon and oxygen isotope analysis has been carried out with samples from the Barranco de las Calzadas section, throughout the upper part of the Forcall Formation where the boundaries between the *Deshayesites weissi*, *Deshayesites deshayesi* and *Dufrenoyia furcata* ammonite biozones have been exactly determined (Moreno-Bedmar et al., 2009, accepted). Hence, this section offers an excellent opportunity to link the characteristic $\delta^{13}C$ perturbations related to the Early Aptian Oceanic Anoxic Event (OAE1a) with high-quality ammonite biostratigraphic data. The C and O isotopic data measured are reported and graphically presented in Fig. 10.

Carbon-isotope data

The carbon-isotope values obtained range between -1.41‰ and 5‰. The resulting $\delta^{13}C_{carb}$ curve has been divided into eight segments (C1-C8; Fig. 10) in order to simplify its analysis and discussion following Menegatti et al. (1998), Bellanca et al. (2002), and de Gea et al. (2003). The lowest part of the C-isotope curve begins in the *Roloboceras hambrovi* horizon (*Deshayesites weissi* biozone) with a slightly negative excursion from 1.02‰ to -0.30‰ (C1), followed by a positive trend to 0.72‰ (C2). Straight afterwards, the $\delta^{13}C_{carb}$ values reach an absolute minimum of -1.41‰ in a sharp negative excursion (C3), with a subsequent well-developed positive shift to 0.72‰ (C4). After this step-like positive excursion, an interval marked by similar C_{carb}-isotopic values ranging between 2.66‰ to

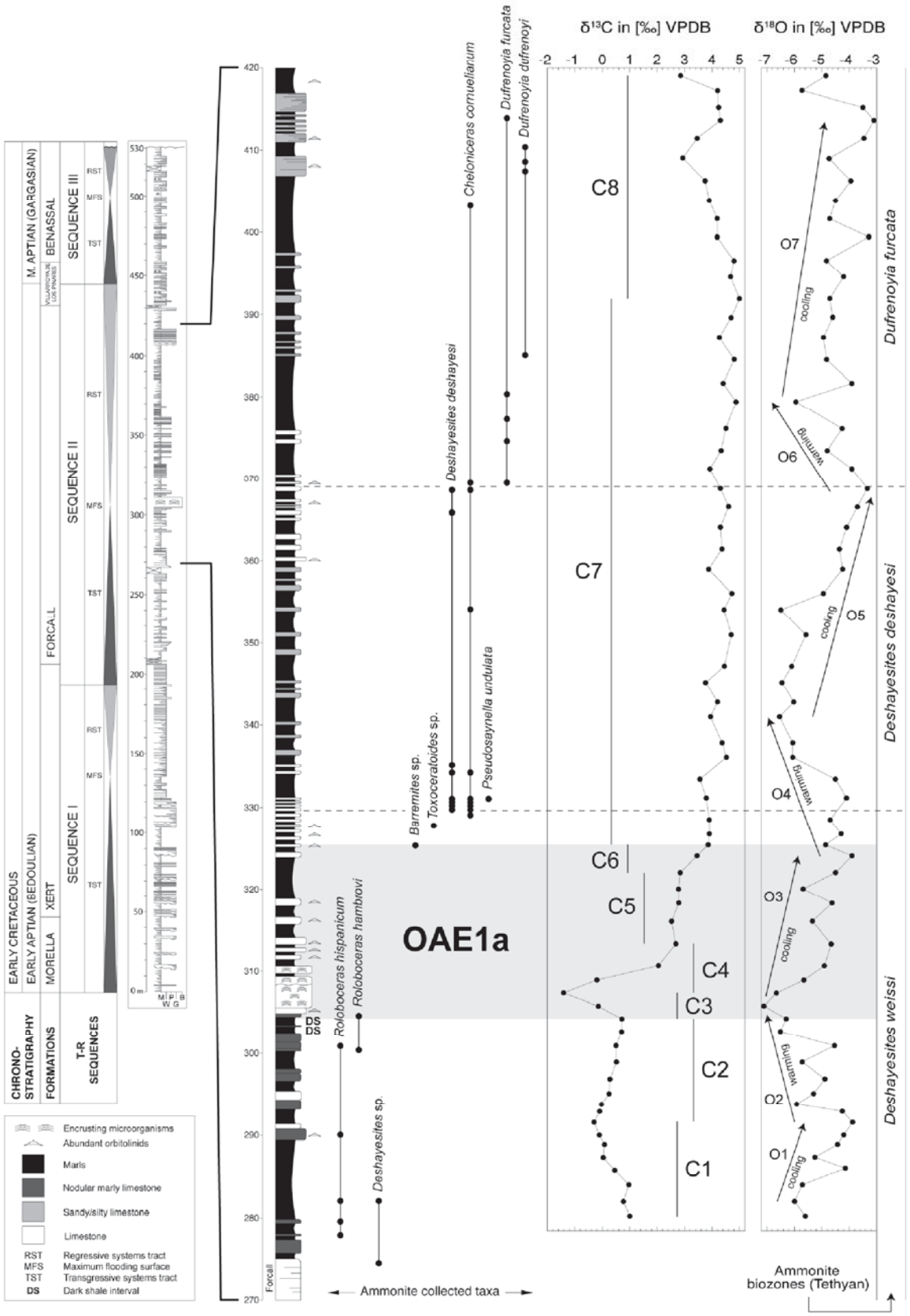

FIGURE 10 | **Detailed section log from Barranco de las Calzadas, featuring carbon- and oxygen-isotope curves, the situation of the OAE1a interval (indicated in grey), and the collected ammonite taxa. Segments C1-C8 and O1-O7 indicate $\delta^{13}C$ and $\delta^{18}O$ trends, respectively. Refer to text for detailed discussion.**

2.83‰ (C5) begins. Then, the curve shows another steep positive shift to 3.85‰ (C6), followed by a large gentle positive trend with many minor reversals that begins before the top of the *Deshayesites weissi* biozone and passes through the entire *Deshayesites deshayesi* biozone into the base of the *Dufrenoyia furcata* biozone, where it reaches an absolute maximum of 5‰ (C7). Subsequently, the $\delta^{13}C_{carb}$ values drop again along the top of the Forcall Formation, where a relative minimum of 2.85‰ is reached (C8).

Oxygen-isotope data

The resulting oxygen-isotope values vary between -7.11‰ and -3.09‰. Despite much fluctuation, seven relative trends indicating cooling-warming tendencies can be interpreted in the isotope curve obtained (O1 to O7; Fig. 10). The $\delta^{18}O$ curve begins inside the *Deshayesites weissi* biozone with a minor positive excursion that may reflect a cooling tendency (O1). This initial positive shift is equivalent to the segment C1. The subsequent trend corresponds to an irregular negative evolution of the oxygen-isotope data that reaches the absolute minimum value of the curve (O2), which could denote a progressive warming episode. This negative trend can be correlated with the segment C2 and the lower part of the segment C3. The third interpreted trend draws a positive shift of the $\delta^{18}O$ values suggesting a cooling event (O3), which is correlatable with the upper part of the segment C3, the segments C4, C5 and the lower part of segment C6. Straight afterwards, the $\delta^{18}O$ curve describes another negative trend indicating a possible warming interval (O4), which comprises the top of the *Deshayesites weissi* biozone and the base of the *Deshayesites deshayesi* biozone, and it is equivalent with the lower part of the segment C7. Then, the curve displays a long positive shift that reaches the top of the *Deshayesites deshayesi* biozone, which may denote a cooler climate (O5), followed by a warming event marked by the subsequent negative excursion that coincides with the lower part of the *Dufrenoyia furcata* biozone (O6). After this shift towards negative values, the $\delta^{18}O$ curve shows a positive tendency that could reflect another cooling time interval (O7), which reaches the absolute maximum O-isotope value inside the lower part of the *Dufrenoyia furcata* biozone. This last shift towards positive $\delta^{18}O$ values is correlatable with the upper part of the segment C7 and the segment C8.

QUANTITATIVE SUBSIDENCE ANALYSIS AND ACCOMMODATION

In the Galve sub-basin, Aptian carbonate and siliciclastic sedimentation was tectonically controlled by the activity of the Miravete transfer fault and five main tilted blocks, which experienced syn-rift differential subsidence and compartmentalised both sides of the sub-basin (Fig. 11A). In the following, the total sediment accommodation for each block is calculated, taking into account total subsidence (with decompaction) and estimated palaeo-water depths (see Material and Methods for details). For this purpose five representative stratigraphic columns, each one belonging to a different block, were selected (Fig. 11A). Despite small magnitude differences, the five calculated total subsidence curves mainly display the same general pattern (Fig. 11B). The western side curves of Camarillas, Barranco de las Calzadas and Villarroya de los Pinares show higher subsidence rates than those of the eastern side, at Las Cubetas and the Estrecho de la Calzada Vieja. These differences can be attributed to the activity of the Miravete master normal transfer fault, which generated a western side hanging-wall and an eastern side foot-wall. In addition, the magnitude of total subsidence also increases towards the basin. On the eastern side, the distal Estrecho de la Calzada Vieja section displays a higher subsidence rate than the proximal Las Cubetas section. Likewise on the western side, the basinal Villarroya de los Pinares section shows a higher magnitude of total subsidence than the more proximal Camarillas and Barranco de las Calzadas sections. However, all five curves display two major differentiated stages of rapid/slow total subsidence (Fig. 11B).

The first stage (R/S1) is characterized by an initial episode of rapid subsidence, associated with significant extension and normal faulting throughout Sequence I and the TST and early RST of Sequence II (125 to approximately 122.8 Ma). Thus, an array of normal faults affecting the last-mentioned depositional sequences (Xert and Forcall formations) can be observed in the area surrounding Villarroya de los Pinares (Fig. 12). This initial phase reflects the highest subsidence rate for the Aptian in the Galve sub-basin, and is followed by a period of decelerating subsidence that includes the late RST of Sequence II, Sequence III and the TST of Sequence IV (approximately 122.8 to approximately 114.2 Ma). The second stage (R2) is marked by a resumption of accelerated subsidence, which comprises the RST of Sequence IV (approximately 114.2-112 Ma). High subsidence rates in the distal curves of Villarroya de los Pinares and the Estrecho de la Calzada Vieja characterize this second rapid subsidence interval (R2), while the proximal curve of Las Cubetas shows minor acceleration of subsidence. In the Villarroya de los Pinares section, normal faulting linked to this interval of rapid subsidence can be observed affecting the lower part of the RST of Sequence IV (Benassal Formation) (Fig. 7B).

The rapid phases of total subsidence correspond to periods of fault activity and reactivation of tilting of blocks (syn-rift subsidence), producing gains of accommodation. The slower episodes of total subsidence in this area indi-

cate local periods of thermal re-equilibration of the crust, heated during fracture phases (see McKenzie, 1978; Salas et al., 2001), so giving rise to losses of accommodation.

DISCUSSION

Diagenetic alteration of stable isotope data

The carbon- and oxygen-isotope data display more negative values than those from other time equivalent-isotope records in the Mid-Pacific Mountains (Jenkyns, 1995), Oman (Vahrenkamp, 1996), Italy and Switzerland (Menegatti et al., 1998), France (Moullade et al., 1998), Greece (Grötsch et al., 1998), Sicily (Bellanca et al., 2002), Spain (de Gea et al., 2003), Switzerland (Wissler et al., 2003) and Portugal (Burla et al., 2008). This discrepancy is consistent with the observation that $\delta^{13}C$ and $\delta^{18}O$ in platform limestones commonly show depleted values compared with those from pelagic environments (see Vahrenkamp, 1996; Grötsch et al., 1998; Immenhauser et al., 2001; Immenhauser et al., 2005; Sattler et al., 2005; Burla et al., 2008). Different authors have explained several mechanisms that can contribute to this fact such as subaerial exposure, euxinic conditions, fresh-water runoff or diagenetic alteration during burial (Scholle and Arthur, 1980; Allan and Matthews, 1982; Marshall, 1992; Patterson and Walter 1994; Menegatti et al., 1998; Sattler et al., 2005).

Generally, low $\delta^{13}C$ and $\delta^{18}O$ compositions of limestones are associated with diagenetic changes, with increased meteoric influence (Allan and Matthews, 1982; Patterson and Walter, 1994). Due to the epeiric nature of the Barranco de las Calzadas succession such diagenetic effects may have been superimposed on the original isotopic signal. Nevertheless, the $\delta^{13}C$ signal is considered not to be strongly affected by such processes in contrast to what happens with the $\delta^{18}O$ signal (see Scholle and Arthur, 1980; Immenhauser et al., 2001). Therefore, and despite the slight negative shift of the C-isotope values, it is commonly admitted that $\delta^{13}C$ records frequently preserve original patterns (Scholle and Arthur, 1980; Menegatti et al., 1998; Burla et al., 2008). Besides, in the Barranco de las Calzadas section, subaerial exposure surfaces have not been observed, and thin sections show no significant diagenetic features. The absence of a strong diagenetic overprint is also demonstrated by the low covariance ($R^2 = 0.0789$) between the $\delta^{13}C$ and $\delta^{18}O$ values (Fig. 13) (see Menegatti et al., 1998; Grötsch et al., 1998; Burla et al., 2008). Therefore, and due to the similarity between the Barranco de las

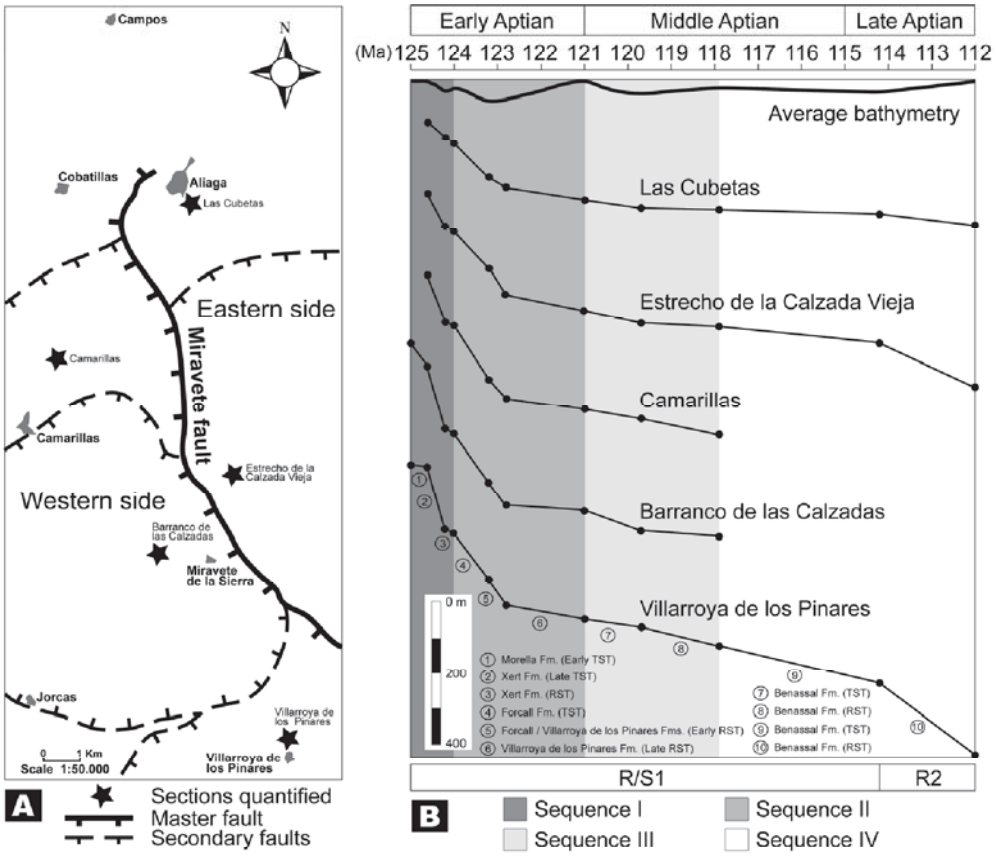

FIGURE 11 | **A) Schematic tectonic map of the Galve sub-basin showing the situation of the different sections used in the quantitative subsidence analysis. B) Decompacted total subsidence curves corrected for palaeobathymetries representing total accommodation. The average bathymetry curve is also indicated. Absolute ages are from Ogg and Ogg (2006). R/S: Stage of rapid/slow total subsidence. R: Stage of rapid total subsidence.**

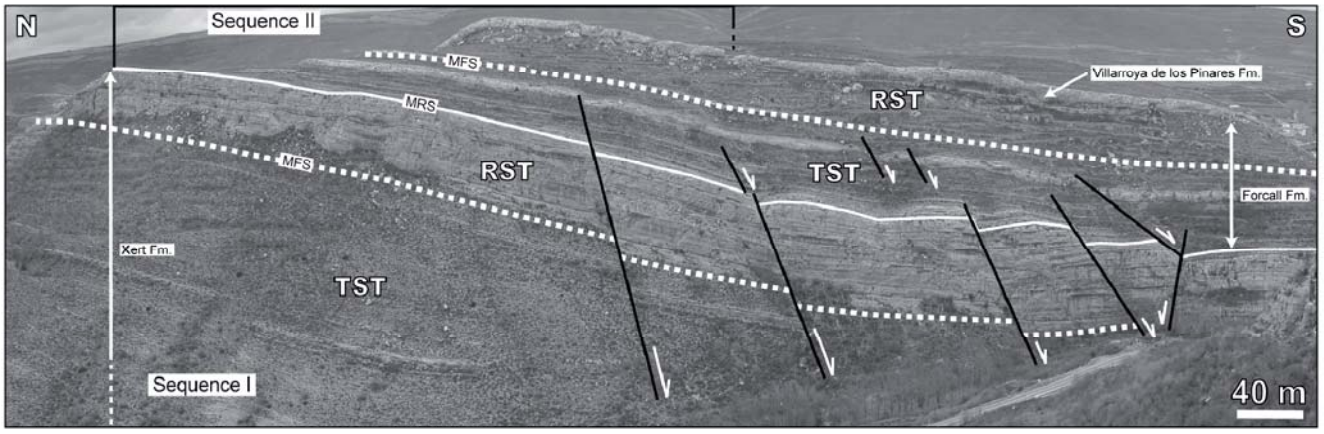

FIGURE 12 | **Photograph of the lower part of the Villarroya de los Pinares section showing an array of synsedimentary normal faults affecting Sequence I and the TST of Sequence II (Xert and Forcall formations). See Fig. 5 for legend.**

Calzadas isotopic patterns and other Early Aptian examples reported, e.g., Vahrenkamp (1996), Menegatti et al. (1998), Bellanca et al. (2002), de Gea et al. (2003), the resulting $\delta^{13}C$ curve is interpreted to reflect global trend fluctuations.

Carbon-isotope record

The C_{carb}-isotopic record of the Barranco de las Calzadas section is subdivided into eight stratigraphic segments (C1-C8; Fig. 10), which are interpreted to reflect globally recognizable patterns (Menegatti et al., 1998; Bellanca et al., 2002; de Gea et al., 2003). Menegatti et al. (1998) defined the Early Aptian oceanic anoxic event (OAE1a; "Livello Selli") chemostratigraphically as the interval comprising the segments C4, C5 and C6 (Fig. 10). Nevertheless, in this paper the OAE1a time span will be interpreted to include the negative spike of segment C3, as well, as established in other recent studies (Fig. 10; see Li et al., 2008; Méhay et al., 2009; Tejada et al., 2009; Millán et al., 2009). This event is globally correlatable and can be identified in many other $\delta^{13}C$ curves (e.g., Vahrenkamp, 1996; Menegatti et al., 1998; Moullade et al., 1998; Bellanca et al., 2002; de Gea et al., 2003; Sattler et al., 2005). The ammonites collected in the Barranco de las Calzadas section permit us to attribute the Early Aptian oceanic anoxic event to the *Roloboceras hambrovi* horizon (upper part of the *Deshayesites weissi* biozone; Fig. 10; see Moreno-Bedmar et al., 2009, accepted).

The C- and O-isotopic analysis carried out by Embry (2005) in the Estrecho de la Calzada Vieja section (eastern side of the Miravete fault) displays two similar positive $\delta^{13}C_{carb}$ excursions (C2 and C4) at the same stratigraphic levels as observed in the Barranco de las Calzadas section (western side of the Miravete fault) but with more positive values. Despite evident diagenetic effects, the two negative-positive spikes (C1-C2 and C3-C4; Fig. 10) of the $\delta^{13}C$ evolution are interpreted to be of global significance, and could be equivalent with the ones observed in La Bédoule section (France; Moullade et al., 1998) and the Mt. Kanala section (Greece; Grötsch et al., 1998). In both cases, the onset of the OAE1a has been ascribed to the second positive shift (C4; Fig. 10). By contrast, Embry (2005) attributed the onset of the OAE1a to the first positive C-isotope excursion (C2 of this study; Fig. 10). However, and as mentioned earlier, in this study the inception of the OAE1a was placed at the negative $\delta^{13}C$ spike of C3 (see Fig. 10) following Li et al. (2008), Méhay et al. (2009), Tejada et al. (2009) and Millán et al. (2009). Although the term oceanic anoxic event is used throughout this work, the presence of diverse and abundant biota throughout the OAE1a time span, suggests oxygenated conditions rather than anoxia, in this area at least.

Oxygen-isotope record

On account of the susceptibility to diagenetic alteration of oxygen isotopes during burial conditions (Scholle and Arthur, 1980; Patterson and Walter, 1994; Menegatti et al., 1998), the $\delta^{18}O$ results are unreliable and display no regular patterns like those observed for the carbon isotopic values. For this reason, the resulting oxygen-isotope data should be treated with caution. However, the low covariance obtained between the $\delta^{13}C$ and $\delta^{18}O$ values (Fig. 13) and the absence of homogeneous $\delta^{18}O$ values or marked persistent saw-tooth-shaped excursions (Fig. 10), may be indicative of only weak diagenetic overprint (see Menegatti et al., 1998; Grötsch et al., 1998; Sattler et al., 2005; Burla et al., 2008). The marly nature of the succession probably diminished fluid circulation, and therefore excluded the possibility of stronger diagenetic effects. Hence, the oxygen-isotope results exhibit a gentle-scattered sinusoidal-shaped curve build-up of seven relative trends (O1 to O7; Fig. 10),

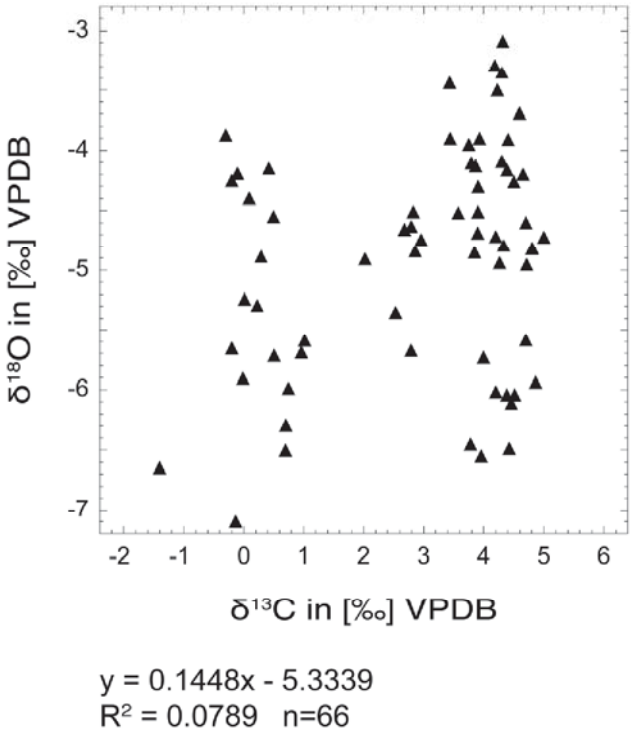

FIGURE 13 | **Cross-plot of $\delta^{13}C$ and $\delta^{18}O$ results. The low covariance between $\delta^{13}C$ and $\delta^{18}O$ ($R^2 = 0.0789$) indicates lack of significant diagenetic overprint.**

which could preserve original high-frequency climatically-driven tendencies.

In this respect, the interpreted segments O2 and O3 (Fig. 10) have been also reported by Menegatti et al., (1998), Hochuli et al., (1999), Bellanca et al., (2002), de Gea et al., (2003) and Ando et al., (2008). The segment O2, which may reflect a warming episode, could be linked to high light carbon concentrations introduced into the ocean-atmosphere system by marine volcanism (Méhay et al., 2009) and/or to massive (isotopically light) methane-release from clathrates (Jenkyns and Wilson, 1999; Jahren et al., 2005; Beerling et al., 2002), peaking in C3 due to greenhouse warming, while segment O3 would reflect a cooling episode resulting from the burial of organic carbon during OAE1a (Fig. 10). Furthermore, the $\delta^{18}O$ curve interval comprising the segments O3 to O7 seems to describe a scattered positive trend through the top of the *Deshayesites weissi* biozone, the *Deshayesites deshayesi* biozone and the lower part of the *Dufrenoyia furcata* biozone, which may also indicate a slow but progressive cooling period, though with a temporary reversal in O4 and O6 (Fig. 10). This shift to a cooler global climate during the late early Aptian has been also reported by Hochuli et al. (1999), in a combined palynological and organic geochemical study in the Cismon section (Italian Alps), Steuber et al. (2005), in a $\delta^{13}C$ and $\delta^{18}O$ study of shells of rudist bivalves from different Tethyan localities, and Ando et al. (2008), in the central Pacific Ocean.

The Aptian evolution of the Galve sub-basin: controlling factors

The sedimentary evolution of the Galve sub-basin during the Aptian was the result of a complex interaction between different local, regional and global factors that controlled the type and rate of sediment production/supply, the available accommodation and how it was filled. These variables mainly concerned extensional faulting linked to the opening of the Atlantic Ocean (Salas et al., 2001), oceanic volcanic/tectonic activity (Larson and Erba, 1999), eustatic variations in sea level, fluctuations in climate and associated environmental consequences. Below, the factors controlling the evolution of the Galve sub-basin are identified and their effect on the composition and nature of the sedimentary record are discussed.

Eustatic sea level change

The durations of the interpreted sequences range from 1 Ma to approximately 5.9 Ma. These estimates are based on available biostratigraphic data and polarity reversals of the geomagnetic field. No substantial sedimentary gaps were identified. However, the boundary between sequences III and IV, which lies in the Middle Aptian time interval, lacks precise age attribution. The fact that sequences I, II, and the upper boundary of Sequence IV seem to correlate rather well with the Aptian global sequences of Ogg and Ogg (2006) (Fig. 14), indicates at least a partial eustatic imprint on Aptian sedimentation in the Galve sub-basin. For the Middle Aptian substage, no significant increase in rift activity has been obtained from the quantitative subsidence analysis (Figs. 11 and 14). Hence, the boundary between the sequences III and IV was probably also a response, at least in part, to eustasy. Consequently, the boundary has been interpreted to be equivalent with that between the Ap4 and Ap5 global sequences of Ogg and Ogg (2006). This interpretation leads to an estimated duration of 3.1 Ma for Sequence III and 5.9 Ma for Sequence IV.

The exact stratigraphic position of the maximum flooding surface in Sequence II is also problematical. Due to the absence of a well-defined correlatable surface marking a large-scale change from a deepening- to a shallowing-up trend, this surface has been placed at the base of the horizon of coral rubble encrusted by *Lithocodium aggregatum* and *Bacinella irregularis*. The latter horizon coincides with the minimum $\delta^{18}O$ values reached at the termination of segment O2 (Figs. 5, 6 and 10). The top of this negative $\delta^{18}O$ shift is thought to mark a thermal maximum and consequently a likely culmination of continental ice melting

leading to a global highstand of relative sea level. However, the occurrence in some parts of the western side of two levels of laminated dark shales below the orbitolinid bed that underlies the encrusted coral rubble horizon may be indicative of dysoxic conditions due to the absence of bioturbation and the presence of preserved organic matter (see Fig. 10). These dark shale episodes probably correspond to the deeper facies recognized throughout Sequence II. Nevertheless, these characteristic intervals were not observed in the eastern side, thus invalidating them as correlatable maximum flooding surface within the sub-basin. Besides, these dark shale levels might only reflect local dysoxic conditions, and not necessarily the expression of the maximum flooding deposit of Sequence II. Whatever the exact position of the maximum flooding surface of Sequence II, both possibilities are situated within the *Roloboceras hambrovi* horizon (upper part of the *Deshayesites weissi* biozone) a little below the position shown for it in the Aptian global sequence Ap3 of Ogg and Ogg (2006), which lies at the limit between the *Deshayesites weissi* and *Deshayesites deshayesi* biozones (Fig. 14).

If this interpretation is correct, these results imply global eustatic sea level changes within a time frame of a few My or less during the Aptian. In this regard, many authors (e.g., Immenhauser, 2005; Gréselle and Pittet, 2005) have suggested glacio-eustasy as the most feasible single known mechanism that could best explain such rapid and significant sea level oscillations. Also Peropadre et al. (2008), in an alternative interpretation of the Aptian sedimentary succession studied here, arrived at the same conclusion. And indeed, over the last couple of decades, several studies have put forward the possibility of the existence of short cooling episodes during the Aptian, which could have favoured the transient presence of small- to moderate-sized ice sheets situated in high altitudes and/or high latitudes (Frakes and Francis, 1988; Weissert and Lini, 1991; Stoll and Schrag, 1996; Price, 1999; Immenhauser, 2005; Gréselle and Pittet, 2005; see also Skelton, 2003b, pp. 172-3). The occurrence of cooling events during this stage is likewise indicated by the oxygen-isotope record presented in this paper. Geochemical analyses reported by Hochuli et al. (1999), Dumitres-

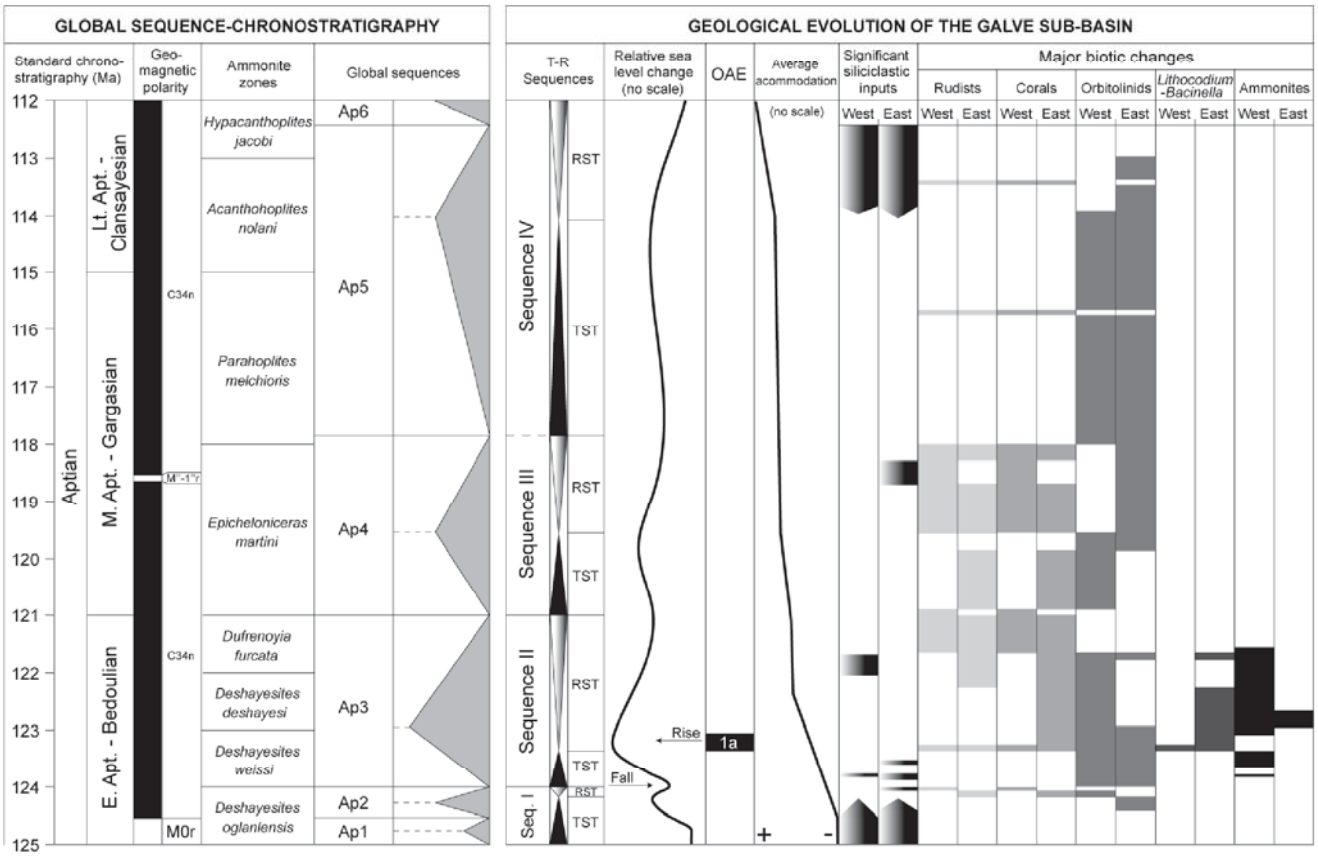

FIGURE 14 | **Comparison chart between the Aptian sequence chronostratigraphy according to Ogg and Ogg (2006), and the Aptian evolution of the Galve sub-basin, with the large-scale T-R sequences, stacking patterns, relative sea level curve, situation of the OAE1a, average accommodation, terrigenous inputs and biotic changes.**

cu et al. (2006), Ando et al. (2008), report similar patterns. Moreover, glacio-eustasy could also explain why many of these relative sea level changes recognized in the Galve sub-basin have been also identified in other coeval Tethyan basins (Fig. 14).

The most remarkable case of significant relative sea level fluctuations is the fall that gave rise to the RST of Sequence II, which resulted in subaerial exposure around latest Early Aptian time at the western hanging-wall side of the Miravete fault (Bover-Arnal et al., 2009). This drop in sea level is interpreted to have been partially eustatic in origin, as no signs of tectonic uplift have been identified in the study area. Furthermore, despite small differences in age, it has been also recognized in the Russian Platform (Sahagian et al., 1996), southern Croatia (Husinec and Jelaska, 2006), the United Arab Emirates (Yose et al., 2006), Oman (Hillgärtner et al., 2003; Gréselle and Pittet, 2005; Rameil et al., under review) and probably along the margin of the Tethys (Ogg and Ogg, 2006). In Oman, as in the western side of the Miravete fault in the Galve sub-basin, the maximum fall in sea level gave rise to forced regressive deposits (Bover-Arnal et al., 2009). Nevertheless, in the Galve sub-basin, conclusive signs of subaerial exposure around the latest Early Aptian in the eastern foot-wall side of the Miravete fault were not recognized. Vennin and Aurell (2001) identified forced regressive deposits and evidence of subaerial processes of late Early Aptian age in this part of the sub-basin, but our field data do not support such an interpretation. Further work needs to be done in this respect. On the other hand, and in line with the foregoing, during the late Early Aptian, the Galve sub-basin apparently experienced decelerating subsidence that, together with an increase of carbonate production and accumulation rates, could also have favoured the shallowing of relative sea level (Fig. 11). For this time interval, the slow rate of total subsidence is supported by the diminution of the accommodation during the late RST of Sequence II (Villarroya de los Pinares Formation). Thus, the small-scale high-frequency sequences or simple sequences (*sensu* Strasser et al., 1999; Vail et al., 1991), which are frequently interpreted to be formed by high-frequency Milankovitch-driven climate changes (e.g., Vail et al., 1991), become thinner towards the top of the RST. This fact has been also observed in the central and oriental sub-basins of the Maestrat Basin.

Notwithstanding the unknown absolute age of the boundary between sequences III and IV, and the small phase-lags of age, when compared with the Aptian global chronostratigraphic sequences of Ogg and Ogg (2006), of the upper boundary of Sequence IV and of the maximum flooding surface of Sequence II, eustasy is apparently one of the main controls on the Aptian sedimentary evolution of the Galve sub-basin (Fig. 14).

Subsidence and faulting

In addition to the influence of eustasy, subsidence also played an important role in creating accommodation throughout the Aptian. Subsidence analysis shows that the fault-controlled rapid syn-rift subsidence registered during Sequence I, the TST and the early RST of Sequence II and the RST of Sequence IV, was the primary factor producing accommodation (Fig. 11). The climax of rifting for the Aptian occurred during Sequence I (Morella and Xert formations with important siliciclastic supplies) and the TST and early RST of Sequence II (Forcall Formation) in which up to 430 m of mixed carbonate-siliciclastic deposits were deposited in approximately 2.2 Ma (the absolute age is based in Ogg and Ogg, 2006) (Figs. 11, 12 and 14). Hence, it is evident that the Aptian sedimentary record of the Galve sub-basin was controlled by both tectonics and eustasy. Despite the high rates of syn-rift subsidence recorded during the Early and the Late Aptian, tectonic activity failed to mask the global eustatic trends. During the Early Aptian, the high rate of syn-rift subsidence probably acted as an amplifier of the widely recognized long-term transgressive context recorded around the Tethys (Föllmi et al., 1994; Sahagian et al., 1996; Weissert et al., 1998; Wissler et al., 2003; Husinec and Jelaska, 2006). On the other hand, the rapid subsidence interval registered towards the basin during the RST of Sequence IV (latest Late Aptian substage) was apparently counterbalanced by enhanced supply and accumulation of terrigenous material that presumably matched the subsidence, permitting the regression recorded around the boundary between the Aptian and the Albian as also seen in other parts of the Tethyan realm (Sahagian et al., 1996; Gréselle and Pittet, 2005; Husinec and Jelaska, 2006).

The four T-R sequences recognized in this study present significant thickness differences between the different sections logged (Figs. 5 and 6). This fact reveals that local differential subsidence within the sub-basin also influenced the distribution of sediment and facies assemblages during the Aptian in this western margin of the Maestrat Basin (Fig. 11). The most striking tectonic feature, the Miravete fault (Fig. 1B), gave rise in its eastern foot-wall side to mostly thinner sequences with facies assemblages reflecting shallower water conditions than on the western hanging-wall side (Figs. 5 and 6). The effects of differential subsidence can also be noted within the eastern side foot-wall where the sequences identified in the Las Cubetas, Cabezo de las Hoyas and Alto del Collado sections are thinner than the same sequences recognized in the Loma del Horcajo and Estrecho de la Calzada Vieja sections (Fig. 5). Nevertheless, the RST of Sequence IV in the proximal Loma del Horcajo, Las Cubetas and Cabezo de las Hoyas sections is significantly thinner than in the distal Estrecho de la Calzada Vieja and Alto del Collado sections; this difference

seems not to be related to syn-sedimentary normal faulting, but may be linked to erosive processes either previous to, or linked with deposition of the Albian coal-bearing Escucha Formation (Fig. 5 and 8). However, this unconformity was recognized only in the Las Cubetas section, where a transgressive ravinement surface was identified. Within the western hanging-wall side of the Miravete fault, the increase in thickness of Sequence I in the Loma del Morrón and Barranco de las Calzadas with respect to the Camarillas section can also be interpreted in terms of differential subsidence. The thickness reduction of this sequence and Sequence II in the distal Barranco del Portolés and Villarroya de los Pinares in comparison with the more proximal sections may be related to basinal starvation (Fig. 6).

Environmental changes and facies succession

It has been shown that the mixed carbonate-siliciclastic Aptian sedimentary succession of the Galve sub-basin was substantially controlled by variations in accommodation linked to relative fluctuations of sea level, of both eustatic and tectonic origin. Carbonate producers, moreover, are also very sensitive to changes of other environmental factors, which mainly control the type of carbonate-producing biota and the amount of carbonate produced. The Aptian has been commonly interpreted as a time interval of strong climatic and oceanographic changes (Weissert and Lini, 1991; Larson and Erba, 1999; Hochuli et al., 1999; Pittet et al., 2002; Wissler et al., 2003; Skelton, 2003b; Weissert and Erba, 2004, among others). These ocean-climate system disturbances must also be considered in order to explain the observed facies succession and the biotic changes recorded throughout the Aptian Stage in the western Maestrat Basin.

In the area studied, the Aptian sedimentary evolution starts with fluvial lowstand deposits with tidal influence (Morella Formation), which become progressively more marine in character upwards in the succession, merging laterally into the Xert Formation. Both formations are marked by important fluxes and accumulation of siliciclastics (Figs. 5, 6 and 14). This significant supply of siliciclastic sediments could have been caused by the high-rate of extensional tectonic activity recorded for this time in the Galve sub-basin (Fig. 11), and the associated erosion in the uplifted areas. These terrigenous inputs possibly brought excess nutrients to the sea, inducing a low rate of carbonate production (see Hallock and Schlager, 1986), and favouring the widespread development of facies dominated by large-sized discoidal orbitolinids, mainly by *Palorbitolina lenticularis*, in the Xert Formation (Figs. 5, 6 and 14) (Vilas et al., 1995; Pittet et al., 2002; Embry, 2005). The diminution of siliciclastic fluxes during the RST of Sequence I may have caused changes in the trophic conditions, lowering the nutrient concentration in the basin and favouring the establishment of incipient carbonate ramps characterized by green algae, miliolids, small requieniid rudists and *Chondrodonta* (Figs. 5 and 6).

Another episode of widespread development of orbitolinids occurred during the TST of Sequence II. This systems tract represents the acme of the overall transgressive context recorded during the Early Aptian throughout the Tethys (Föllmi et al., 1994; Sahagian et al., 1996; Wissler et al., 2003; Husinec and Jelaska, 2006). Further, as discussed already, this sea level rise was amplified in the Galve sub-basin by local rapid syn-rift subsidence (Figs. 11 and 14). The magnitude of this transgressive phase was larger than that recorded in Sequence I, and together with intensified greenhouse conditions and consequently, an acceleration of the hydrological cycle, probably triggered by major volcanic events in the Pacific Ocean, might have provoked another episode of significant nutrient influx into the basin (Weissert et al. 1998; Larson and Erba, 1999). This event caused the drowning of the incipient carbonate platforms with small requieniid rudists, *Chondrodonta*, miliolids and green algae established during the regressive phase of Sequence I (upper part of the Xert Formation), and the widespread development of large-sized discoidal *Palorbitolina lenticularis* beds throughout the Forcall Formation. The latter transgression moved the littoral belt further landwards and, with it, the source of siliciclastic supply. However, silt-sized siliciclastic particles still arrived in the basin. The widespread development of orbitolinids during the Early Aptian in the Galve sub-basin has already been discussed by Embry (2005), who linked it with the overall occurrence of orbitolinid beds around the Tethyan realm during the Early Aptian broad transgression (Vilas et al., 1995; Pittet et al., 2002; Burla et al., 2008).

The marly deposits interbedded with marly limestones and limestones rich in orbitolinids that characterize the TST of Sequence II (Forcall Formation) are interrupted by amalgamated episodes of coral rubble encrusted by *Lithocodium aggregatum* and *Bacinella irregularis*. The base of this encrusted coral rubble horizon is distinguished by the presence of resedimented *Palorbitolina lenticularis* with large flat morphologies in rock-forming abundance. These characteristic deposits are synchronous with the widely recognized $\delta^{13}C$ negative spike that marks the onset of OAE1a and the lower part of the succeeding positive carbon-isotope excursion, as well as with the warming-cooling trends (O2 and O3) associated with these events (Fig. 10). The fact that these lithofacies dominated by *Lithocodium-Bacinella* include significant terrigenous inputs, evidence of strong bioerosion (Hallock and Schlager, 1986) and large-sized discoidal *Palorbitolina lenticularis* suggests that they were developed under nutrient-rich conditions (Vilas et al., 1995; Pittet et al., 2002). The base of these encrusted coral debris deposits also coincides with

the minimum $\delta^{18}O$ value reached throughout the Barranco de las Calzadas section (Fig. 10). This absolute minimum value of the oxygen-isotope curve might have been linked to intensified greenhouse conditions and thus to the maximum flooding surface of Sequence II, due to the minimum presence of continental ice, as well as to increased humidity, weathering and erosion resulting in enhanced land-ocean nutrient fluxes. In Oman, Immenhauser et al. (2005) already noted the possible relation between the problematical *Lithocodium-Bacinella* association and the OAE1a, as well as a probable linkage of these facies with high trophic levels (see also Rameil et al., 2010). Furthermore, several authors have also related the OAE1a and episodes of transgression within the Early Aptian with elevated nutrient levels in the sea (Föllmi et al., 1994; Erba, 1994; Weissert et al., 1998; Weissert and Erba, 2004). In addition, elevated seawater temperatures and changes in ocean water chemistry such as acidification triggered by the aforementioned global warming event that may have led to the OAE1a could also have played a part in favouring the generation of coral rubble and the widespread development of *Lithocodium-Bacinella* facies (see also Hillgärtner et al., 2003; Immenhauser et al., 2005; Rameil et al., 2010).

On the other hand, just after the inception of the OAE1a, a long progressive cooling period began (Fig. 10), also recognized in other regions of the Tethys (Hochuli et al., 1999; Bellanca et al., 2002; Steuber et al., 2005; Ando et al., 2008, among others), and a long-term regressive phase that ended around the boundary between the Aptian and the Albian occurred (Fig. 14). This long-term regressive phase, spanning the late Early Aptian, and the Middle and Late Aptian substages, has been also described around the Neo-Tethys (e.g., Husinec and Jelaska, 2006). On the eastern side of the Miravete fault (foot-wall block), above the level of the carbon-isotope perturbations corresponding to the OAE1a and associated with the aforementioned progressive regression of relative sea level, a large carbonate platform with corals and rudists developed during the *Deshayesites deshayesi* and *Dufrenoyia furcata* biozones, giving rise to the RST of Sequence II (Villarroya de los Pinares Formation) (Fig. 5). On the western side (hanging-wall block), the sedimentary succession, which consists of green marls with interbedded limestones, marly limestones and silty limestones with abundant orbitolinids and ammonites, indicates that bathymetry was probably too significant to permit the establishment of carbonate platforms. However, during the upper part of the *Dufrenoyia furcata* biozone (late Early Aptian), and linked with the subsequent lowering of sea level, a large carbonate platform dominated by *Toucasia carinata*, *Polyconites* new species (Skelton et al., in press) and corals (Villarroya de los Pinares Formation) developed in the proximal setting of this side (Fig. 6).

All these carbonate systems drowned with the TST of Sequence III, mainly evolving to marly sediments with calcareous nodules and orbitolinids (Benassal Formation). During the following RST carbonate production was able to recover in both sides of the Miravete fault. However, during this regressive episode inputs and accumulation of siliciclastic materials occurred in proximal areas of the eastern side of the Miravete fault during an interval of decelerating subsidence (Figs. 11 and 14). These siliciclastic events on the eastern side of the Miravete fault, which are interpreted to have been linked with enhanced weathering on the continents caused by a long-term rise in humidity that prevailed from the Middle to Late Aptian (Ruffell and Worden, 2000), might have shut down the carbonate factories and provoked the development of orbitolinid-rich deposits at certain times. The subsequent transgression (TST of Sequence IV) moved the siliciclastic belt landwards and caused the definitive drowning of these Middle Aptian carbonate platforms.

The major siliciclastic influx for the Aptian in the Galve sub-basin generated the RST of Sequence IV (Figs. 5, 6 and 14). This event favoured once again the development of orbitolinid beds, in the basal part of this regressive phase, followed by the establishment of littoral conditions rich in terrigenous sediments. For the RST of Sequence IV, only two small incipient carbonate platforms of corals and rudists were recognized on both sides of the Miravete fault. These carbonate factories were rapidly shut down by the high current energy conditions and input of siliciclastics that characterized the latest Aptian. This major terrigenous episode close to the boundary between the Aptian and the Albian occurred during the acme of the regression that began in the late Early Aptian. This siliciclastic event was probably triggered by resumption of the rapid syn-rift subsidence (Figs. 11 and 14), coupled with an intensified humid climate (Ruffell and Worden, 2000), which could have significantly increased chemical weathering on continents and runoff during the latest Aptian.

CONCLUSIONS

The Aptian stratigraphic record of the western Maestrat Basin is an instructive example of a terrigenous-influenced carbonate system controlled by both regional tectonic factors and global ocean-climate changes. This sedimentary record can be subdivided into four T-R sequences reflecting long-term relative sea level variations: i) Sequence I (lowermost Aptian); ii) Sequence II (Lower Aptian); iii) Sequence III (Middle Aptian); and iv) Sequence IV (Middle-Upper Aptian). The transgressive systems tracts of these sequences are dominated by alternations of marls and limestones rich in orbitolinids, while the regressive systems tracts essentially consist of wave- and tidally influenced siliciclastic

and carbonate deposits, and by the development of carbonate platforms with rudist bivalves, corals, orbitolinids and green algae. Three types of carbonate platforms were identified: i) homoclinal ramp (lowermost Aptian of the eastern and western sides of the Miravete fault); ii) distally steepened ramp (Lower Aptian of the eastern side of the Miravete fault); and iii) flat-topped non-rimmed shelf (Lower Aptian of the western side of the Miravete fault).

Throughout the evolution of this sedimentary system, syn-rift subsidence was the most important provider of accommodation, though it failed to mask global eustatic trends. Accordingly, the T-R sequences and relative sea level changes interpreted for the Aptian of the Galve sub-basin are consistent with the global sequences and inferred rises and falls of relative sea level recorded in other coeval Tethyan basins, as well as with the major environmental changes discussed in the literature for this time slice. The Aptian sedimentary succession of the western Maestrat Basin thus reflects the following components.

i) a transgression of Early Aptian age accompanied by the widespread development of *Palorbitolina lenticularis* beds associated with the probable intensified greenhouse conditions and enhanced terrigenous influxes that may have led to the OAE1a. Carbon-isotope analysis shows that the negative $\delta^{13}C$ spike that marks the onset of the OAE1a lies in the *Deshayesites weissi* ammonite biozone and is coincident with a horizon of coral rubble encrusted by *Lithocodium aggregatum* and *Bacinella irregularis*, and abundant large-sized discoidal *Palorbitolina lenticularis*. The $\delta^{18}O$ curve seems to reflect high-frequency climatically-driven cyclicity and displays a warming trend that ends around the inception of the OAE1a. This is followed by a subsequent long-term progressive cooling episode throughout the late Early Aptian, which was accompanied by regression characterized by the establishment of a large carbonate platform with typical Urgonian biotic associations dominated by rudist bivalves and corals.

ii) a latest Early Aptian forced regression of relative sea level that ended in subaerial exposure of the carbonate platform that had developed during the late Early Aptian, and in the basinward deposition of forced regressive wedges.

iii) a late Early to Late Aptian long-term regressive phase, which gave rise to the installation of littoral conditions during the Late Aptian with enhanced terrigenous supply, which were probably related to regional tectonics and to a climate progressively changing from a semi-arid regime during the Early Aptian, to a semi-humid mode in the Middle-Late Aptian.

A close interaction between global environmental factors including eustatic trends, regional tectonics and sedimentary and biological succession can thus be observed in the Aptian rocks of the western Maestrat Basin. Consequently, due to the expanded and relatively complete nature of the sedimentary succession reported here, the present study constitutes an outstanding record of changing Aptian conditions of considerable potential value for the analysis, comparison, calibration and better understanding of other time-equivalent epicontinental sedimentary records.

ACKNOWLEDGMENTS

We are grateful to Marc Aurell, Ramón Mas, Niels Rameil and the editor Lluís Cabrera who critically read the manuscript and offered useful suggestions. Rolf Schroeder is sincerely thanked for determining the orbitolinid species. We also thank Miquel Company for his valuable comments on the ammonite biostratigraphy. Roger Clavera-Gispert and Richard Regner are acknowledged for their helpful contributions during the writing of this study. Luis Pomar and Peter van der Beek read a first version of the manuscript. Financial support for the research was provided by the project Bi 1074/1-2 of the Deutsche Forschungsgemeinschaft, by the I+D+i research projects: CGL2005-07445-CO3-01, CGL2008-04916 and CGL2006-02153, by the Consolider-Ingenio 2010 programme, under CSD 2006-0004 "Topo-Iberia", by the Grup Consolidat de Recerca "Geologia Sedimentària" (2005SGR-00890 and 2009SGR-1451), and by the Departament d'Universitats, Recerca i Societat de la Informació de la Generalitat de Catalunya i del Fons Social Europeu.

REFERENCES

Allan, J.R., Matthews, R.K., 1982. Isotope signatures associated with early meteoric diagenesis. Sedimentology, 29, 797-817.

Ando, A., Kaiho, K., Kawahata, H., Kakegawa, T., 2008. Timing and magnitude of early Aptian extreme warming: Unraveling primary $\delta^{18}O$ variation in indurated pelagic carbonates at Deep Sea Drilling Project Site 463, central Pacific Ocean. Palaeogeography, Palaeoclimatology, Palaeoecology, 260, 463-476.

Beerling, D.J., Lomas, M.R., Gröcke, D.R., 2002. On the nature of methane gas-hydrate dissociation during the Toarcian and Aptian oceanic anoxic events. American Journal of Science, 302, 28-49.

Bellanca, A., Erba, E., Neri, R., Premoli Silva, I., Sprovieri, M., Tremolada, F., Verga, D., 2002. Palaeoceanographic significance of the Tethyan 'Livello Selli" (Early Aptian) from the Hybla Formation, northwestern Sicily: biostratigraphy and high-resolution chemostratigraphic records. Palaeogeography, Palaeoclimatology, Palaeoecology, 185, 175-196.

Bogdanova, T.N., Tovbina, S.Z., 1994. On development of the Aptian Ammonite zonal standard for the Mediterranean region. Géologie Alpine, Mémoire Hors Serie, 20, 51-59.

Bond, G.C., Kominz, M.A., 1984. Construction of tectonic subsidence curves for the early Paleozoic miogeocline, southern

Canadian Rocky Mountains: Implications for subsidence mechanisms, age of break-up, and crustal thinning. Geological Society of America Bulletin, 95, 155-173.

Bover-Arnal, T., Moreno-Bedmar, J.A., Salas, R., Bitzer, K., 2008. Facies architecture of the late Early-Middle Aptian carbonate platform in the western Maestrat basin (Eastern Iberian Chain). Geo-Temas, 10, 115-118.

Bover-Arnal, T., Salas, R., Moreno-Bedmar, J.A., Bitzer, K., 2009. Sequence stratigraphy and architecture of a late Early-Middle Aptian carbonate platform succession from the western Maestrat Basin (Iberian Chain, Spain). Sedimentary Geology, 219, 280-301.

Burla, S., Heimhofer, U., Hochuli, P.A., Weissert, H., Skelton, P., 2008. Changes in sedimentary patterns of coastal and deep-sea successions from the North Atlantic (Portugal) linked to Early Cretaceous environmental change. Palaeogeography, Palaeoclimatology, Palaeoecology, 257, 38-57.

Canérot, J., Crespo, A., Navarro, D., 1979. Montalbán 1:50.000, hoja nº 518. Mapa Geológico de España, 2ª Serie, 1ª Edición. Servicio de Publicaciones, Madrid, Ministerio de Industria y Energía, 31pp.

Canérot, J., Cugny, P., Pardo, G., Salas, R., Villena, J., 1982. Ibérica Central-Maestrazgo. In: García, A. (ed.). El Cretácico de España. Universidad Complutense de Madrid, 273-344.

Catuneanu, O., Abreu, V., Bhattacharya, J.P., Blum, M.D., Dalrymple, R.W., Eriksson, P.G., Fielding, C.R., Fisher, W.L., Galloway, W.E., Gibling, M.R., Giles, K.A., Holbrook, J.M., Jordan, R., Kendall, C.G.St.C., Macurda, B., Martinsen, O.J., Miall, A.D., Neal, J.E., Nummedal, D., Pomar, L., Posamentier, H.W., Pratt, B.R., Sarg, J.F., Shanley, K.W., Steel, R.J., Strasser, A., Tucker, M.E., Winker, C., 2009. Towards the standardization of sequence stratigraphy. Earth-Science Reviews, 92, 1-33.

de Gea, G.A., Castro, J.M., Aguado, R., Ruiz-Ortiz, P.A., Company, M., 2003. Lower Aptian carbon isotope stratigraphy from a distal carbonate shelf setting: the Cau section, Prebetic zone, SE Spain. Palaeogeography, Palaeoclimatology, Palaeoecology, 200, 207-219.

Dumitrescu, M., Brassell, S.C., Schouten, S., Hopmans, E.C., Sinninghe Damsté, J.S., 2006. Instability in tropical Pacific sea-surface temperatures during the early Aptian. Geology, 34, 833-836.

Embry, A.F., Klovan, J.E., 1971. A Late Devonian reef tract on northeastern Banks Island, N.W.T. Bulletin of Canadian Petroleum Geology, 19, 730-781.

Embry, J.C., 2005. Paléoécologie et architecture stratigraphique en haute résolution des platesformes carbonatées du Barrémien-Aptien de la Néo-Téthys (Espagne, Suisse, Provence, Vercors) – impact respectif des différents facteurs de contrôle. Doctoral Thesis. Paris, Museum National d'Histoire Naturelle – Institut Français du Petrole, 299pp.

Erba, E., 1994. Nannofossils and superplumes: The early Aptian "nannofossil crisis". Paleoceanography, 9, 483-501.

Föllmi, K.B., Weissert, H., Bisping, M., Funk, H., 1994. Phosphogenesis, carbon-isotope stratigraphy, and carbonate-platform evolution along the Lower Cretaceous northern Tethyan margin. Geological Society of America Bulletin, 106, 729-746.

Föllmi, K.B., Godet, A., Bodin, S., Linder, P., 2006. Interactions between environmental change and shallow water carbonate buildup along the northern Tethyan margin and their impact on the Early Cretaceous carbon isotope record. Paleoceanography, 21, PA4211, doi: 10.1029/2006PA001313.

Frakes, L.A., Francis, J.E., 1988. A guide to Phanerozoic cold polar climates from high-latitude ice-rafting in the Cretaceous. Nature, 333, 547-549.

Gautier, F., 1980. Villarluengo 1:50.000, hoja nº 543. Mapa Geológico de España, 2ª Serie, 1ª Edición, Servicio de Publicaciones, Madrid, Ministerio de Industria y Energía, 45pp.

Gréselle, B., Pittet, B., 2005. Fringing carbonate platforms at the Arabian Plate margin in northern Oman during the Late Aptian-Middle Albian: Evidence for high-amplitude sea-level changes. Sedimentary Geology, 175, 367-390.

Grötsch, J., Billing, I., Vahrenkamp, V., 1998. Carbon-isotope stratigraphy in shallow-water carbonates: implications for Cretaceous black-shale deposition. Sedimentology, 45, 623-634.

Hallock, P., Schlager, W., 1986. Nutrient excess and the demise of coral reefs and carbonate platforms. Palaios, 1, 389-398.

Hillgärtner, H., Van Buchem, F.S.P., Gaumet, F., Razin, P., Pittet, B., Grötsch, J., Droste, H., 2003. The Barremian-Aptian evolution of the eastern Arabian carbonate platform margin (northern Oman). Journal of Sedimentary Research, 73, 756-773.

Hochuli, P.A., Menegatti, A.P., Weissert, H., Riva, A., Erba, E., Premoli Silva, I., 1999. Episodes of high productivity and cooling in the early Aptian Alpine Tethys. Geology, 27, 657-660.

Hunt, D., Tucker, M.E., 1992. Stranded parasequences and the forced regressive wedge systems tract: deposition during base-level fall. Sedimentary Geology, 81, 1-9.

Husinec, A., Jelaska, V., 2006. Relative sea-level changes recorded on an isolated carbonate platform: Tithonian to Cenomanian succession, Southern Croatia. Journal of Sedimentary Research, 76, 1120-1136.

Immenhauser, A., Van der Kooij, B., Van Vliet, A., Schlager, W., Scott, R.W., 2001. An ocean-facing Aptian-Albian carbonate margin, Oman. Sedimentology, 48, 1187-1207.

Immenhauser, A., 2005. High-rate sea-level change during the Mesozoic: New approaches to an old problem. Sedimentary Geology, 175, 277-296.

Immenhauser, A., Hillgärtner, H., Van Bentum, E., 2005. Microbial-foraminiferal episodes in the Early Aptian of the southern Tethyan margin: ecological significance and possible relation to oceanic anoxic event 1a. Sedimentology, 52, 77-99.

Jahren, A.H., Conrad, C.P., Arens, N.C., Mora, G., Lithgow-Bertelloni, C., 2005. A plate tectonic mechanism for methane hydrate release along subduction zones. Earth and Planetary Science Letters, 236, 691-704.

Jenkyns, H.C., 1995. Carbon-isotope stratigraphy and paleoceanographic significance of the Lower Cretaceous shallow-

water carbonates of Resolution Guyot, Mid-Pacific Mountains. In: Winterer, E.L., Sager, W.W., Firth, J.V., Sinton, J.M. (eds.). Proceedings of the Ocean Drilling Program, Scientific Results, 143, 99-104.

Jenkyns, H.C., Wilson, P.A., 1999. Stratigraphy, paleoceanography, and evolution of Cretaceous Pacific guyots: relics from a greenhouse Earth. American Journal of Science, 299, 341-392.

Larson, R.L., Erba, E., 1999. Onset of the mid-Cretaceous greenhouse in the Barremian-Aptian: Igneous events and the biological, sedimentary, and geochemical responses. Paleoceanography, 14, 663-678.

Li, Y-X., Bralower, T.J., Montañez, I.P., Osleger, D.A., Arthur, M.A., Bice, D.M., Herbert, T.D., Erba, E., Premoli Silva, I., 2008. Toward an orbital chronology for the early Aptian Oceanic Anoxic Event (OAE1a, ~120 Ma). Earth and Planetary Science Letters, 271, 88-100.

Liesa, C.L., Soria, A.R., Meléndez, N., Meléndez, A., 2006. Extensional fault control on the sedimentation patterns in a continental rift basin: El Castellar Formation, Galve sub-basin, Spain. Journal of the Geological Society, London, 163, 487-498.

Malchus, N., Pons, J.M., Salas, R., 1996. Rudist distribution in the lower Aptian shallow platform of la Mola de Xert, Eastern Iberian Range, NE Spain. Revista Mexicana de Ciencias Geológicas, 12, 224-235.

Marshall, J.D., 1992. Climatic and oceanographic isotopic signals from the carbonate rock record and their preservation. Geologic Magazine, 129, 143-160.

McKenzie, D., 1978. Some remarks on the development of sedimentary basins. Earth and Planetary Science Letters, 40, 25-32.

Méhay, S., Keller, C.E., Bernasconi, S.M., Weissert, H., Erba, E., Botín, C., Hochuli, P.A., 2009. A volcanic CO_2 pulse triggered the Cretaceous Oceanic Anoxic Event 1a and a biocalcification crisis. Geology, 37, 819-822.

Menegatti, A.P., Weissert, H., Brown, R.S., Tyson, R.V., Farrimond, P., Strasser, A., Caron, M., 1998. High-resolution $\delta^{13}C$ stratigraphy through the early Aptian "Livello Selli" of the Alpine Tethys. Paleoceanography, 13, 530-545.

Millán, M.I., Fernández-Mendiola, P.A., García-Mondéjar, J., 2007. Pulsos de inundación marina en la terminación de una plataforma carbonatada (Aptiense inferior de Aralar, Cuenca Vasco-Cantábrica). Geogaceta, 41, 127-130.

Millán, M.I., Weissert, H.J., Fernández-Mendiola, P.A., García-Mondéjar, J., 2009. Impact of Early Aptian carbon cycle perturbations on evolution of a marine shelf system in the Basque-Cantabrian Basin (Aralar, N Spain). Earth and Planetary Science Letters, 287, 392-401.

Moullade, M., Kuhnt, W., Bergen, J.A., Masse, J.P., Tronchetti, G., 1998. Correlation of biostratigraphic and stable isotope events in the Aptian historical stratotype of La Bédoule (Southeast France). Paris, Comptes-Rendus de l'Académie des Sciences, 327(Serie II), 693-698.

Moreno-Bedmar, J.A., Bulot, L., Latil, J.L., Martínez, R., Ferrer, O., Bover-Arnal, T., Salas, R., 2008. Precisiones sobre la edad de la base de la Fm. Escucha, mediante ammonoideos, en la subcuenca de la Salzedella, Cuenca del Maestrat (E Cordillera Ibérica). Geo-Temas, 10, 1269-1272.

Moreno-Bedmar, J.A., Company, M., Bover-Arnal, T., Salas, R., Delanoy, G., Martínez, R., Grauges, A., 2009. Biostratigraphic characterization by means of ammonoids of the lower Aptian Oceanic Anoxic Event (OAE1a) in the eastern Iberian Chain (Maestrat Basin, eastern Spain). Cretaceous Research, 30, 864-872.

Moreno-Bedmar, J.A., Company, M., Bover-Arnal, T., Salas, R., Delanoy, G., Maurrasse, F.J., Grauges, A., Martínez, R., accepted. Lower Aptian ammonite biostratigraphy in the Maestrat Basin (Eastern Iberian Chain, Spain). Geologica Acta, 8/3, 281-299.

Ogg, J.G., Ogg, G., 2006. Early Cretaceous (103-138 Ma timeslice). Update to: Gradstein, F.M., Ogg, J.G., Smith, A.G., 2004. A Geologic Time Scale. Cambridge University Press, 589pp. Website: http://www.nhm.uio.no/norges/timescale

Patterson, W.P., Walter, L.M., 1994. Depletion of ^{13}C in seawater ΣCO_2 on modern carbonate platforms: Significance for the carbon isotopic record of carbonates. Geology, 22, 885-888.

Peropadre, C., Meléndez, N., Liesa, C.L., 2008. Variaciones del nivel del mar registradas como valles incisos en la Formación Villarroya de los Pinares en la subcuenca de Galve (Teruel, Cordillera Ibérica). Geo-Temas, 10, 167-170.

Pittet, B., Van Buchem, F.S.P., Hillgärtner, H., Razin, P., Grötsch, J., Droste, H., 2002. Ecological succession, palaeoenvironmental change, and depositional sequences of Barremian-Aptian shallow-water carbonates in northern Oman. Sedimentology, 49, 555-581.

Pomar, L., Kendall, C.G.St.C., 2007. Architecture of carbonate platforms: A response to hydrodynamics and evolving ecology. In: Lukasik, J., Simo, A. (eds.). Controls on Carbonate Platform and Reef Development. Society for Sedimentary Geology (SEPM), 89(Special Publication), 187-216.

Price, G.D., 1999. The evidence and implications of polar ice during the Mesozoic. Earth-Science Reviews, 48, 183-210.

Rameil, N., Immenhauser, A., Csoma, A.É., Warrlich, G., under review. Surfaces with a long history: The Aptian top Shu'aiba Formation unconformity, Sultanate of Oman. Sedimentology.

Rameil, N., Immenhauser, A., Warrlich, G., Hillgärtner, H., Droste, H.J., 2010. Morphological patterns of Aptian *Lithocodium-Bacinella* geobodies–relation to environment and scale. Sedimentology, 57, 883-911.

Rosales, I., 1999. Controls on carbonate-platform evolution on active fault blocks: the Lower Cretaceous Castro Urdiales platform (Aptian-Albian, northern Spain). Journal of Sedimentary Research, 69, 447-465.

Ruffell, A., Worden, R., 2000. Palaeoclimate analysis using spectral gamma-ray data from the Aptian (Cretaceous) of southern England and southern France. Palaeogeography, Palaeoclimatology, Palaeoecology, 155, 265-283.

Sahagian, D., Pinous, O., Olferiev, A., Zakharov, V., 1996. Eustatic curve for the Middle Jurassic-Cretaceous based on Russian Platform and Siberian stratigraphy: zonal resolution.

American Association of Petroleum Geologists (AAPG) Bulletin, 80, 1433-1458.

Salas, R., 1987. El Malm i el Cretaci inferior entre el Massís de Garraf i la Serra d'Espadà. Analisi de Conca. Doctoral Thesis. Universitat de Barcelona, 345pp.

Salas, R., Guimerà, J., 1996. Rasgos estructurales principales de la cuenca cretácica inferior del Maestrazgo (Cordillera Ibérica oriental). Geogaceta, 20, 1704-1706.

Salas, R., Guimerà, J., Mas, R., Martín-Closas, C., Meléndez, A., Alonso, A., 2001. Evolution of the Mesozoic Central Iberian Rift System and its Cainozoic inversion (Iberian Chain). In: Ziegler, P.A., Cavazza, W., Roberston, A.H.F., Crasquin-Soleau, S. (eds.). Peri-Tethys Memoir 6: Peri-Tethyan Rift/Wrench Basins and Passive Margins. Paris, Mémoires du Muséum National d'Histoire Naturelle, 186, 145-186.

Salas, R., Martín-Closas, C., Delclòs, X., Guimerà, J., Caja, M.A., Mas, R., 2005. Factores principales de control de la sedimentación y los cambios bióticos durante el tránsito Jurásico-Cretácico en la Cadena Ibérica. Geogaceta, 38, 15-18.

Sattler, U., Immenhauser, A., Hillgärtner, H., Esteban, M., 2005. Characterization, lateral variability and lateral extent of discontinuity surfaces on a Carbonate Platform (Barremian to Lower Aptian, Oman). Sedimentology, 52, 339-361.

Schmoker, J.W., Halley, R.B., 1982. Carbonate porosity versus depth: a predictable relation for south Florida. American Association of Petroleum Geologists (AAPG) Bulletin, 66, 2561-2570.

Scholle, P.A., Arthur, M.A., 1980. Carbone isotope fluctuations in Cretaceous pelagic limestones: potential stratigraphic and petroleum exploration tool. American Association of Petroleum Geologists (AAPG) Bulletin, 64, 67-87.

Sclater, J.G., Christie, P.A.F., 1980. Continental stretching: an explanation of the post-mid-Cretaceous subsidence of the central North Sea Basin. Journal of Geophysical Research, 85, 3711-3739.

Simón, J.L., Liesa, C.L., Soria, A.R., 1998. Un sistema de fallas normales sinsedimentarias en las unidades de facies Urgon de Aliaga. Geogaceta, 24, 291-294.

Skelton, P.W., 2003a. Rudist evolution and extinction - a north African perspective. In: Gili, E., Negra, M., Skelton, P.W. (eds.). North African Cretaceous Carbonate Platform Systems. The North Atlantic Treaty Organization (NATO), Science Series IV: Earth and Environmental Sciences, Kluwer Academic Publishers, 28, 215-227.

Skelton, P.W., 2003b. The Cretaceous World. Cambridge, Cambridge University Press, 360pp.

Skelton, P.W., Gili, E., Bover-Arnal, T., Salas, R., Moreno-Bedmar, J.A., in press. A new species of *Polyconites* from the Lower Aptian of Iberia and the early evolution of polyconitid rudists. Turkish Journal of Earth Sciences.

Soria, A.R., 1997. La sedimentación en las cuencas marginales del surco Ibérico durante el Cretácico inferior y su control estructural. Doctoral Thesis. Universidad de Zaragoza, 363pp.

Steuber, T., Rauch, M., Masse, J.-P., Graaf, J., Malkoc, M., 2005. Low-latitude seasonality of Cretaceous temperatures in warm and cold episodes. Nature, 437, 1341-1344.

Stoll, H.M., Schrag, D.P., 1996. Evidence for glacial control of rapid sea level changes in the Early Cretaceous. Science, 272, 1771-1774.

Strasser, A., Pittet, B., Hillgärtner, H., Pasquier, J-B., 1999. Depositional sequences in shallow carbonate-dominated sedimentary systems: concepts for a high-resolution analysis. Sedimentary Geology, 128, 201-221.

Tejada, M.L.G., Suzuki, K., Kuroda, J., Coccioni, R., Mahoney, J.J., Ohkouchi, N., Sakamoto, T., Tatsumi, Y., 2009. Ontong Java Plateau eruption as a trigger for the early Aptian oceanic anoxic event. Geology, 37, 855-858.

Tomás, S., Löser, H., Salas, R., 2008. Low-light and nutrient-rich coral assemblages in an Upper Aptian carbonate platform of the southern Maestrat Basin (Iberian Chain, eastern Spain). Cretaceous Research, 29, 509-534.

Vahrenkamp, V.C., 1996. Carbon isotope stratigraphy of the upper Kharaib and Shuaiba Formations: implications for the Early Cretaceous evolution of the Arabian Gulf region. American Association of Petroleum Geologists (AAPG) Bulletin, 80, 647-662.

Van Wagoner, J.C., Posamentier, H.W., Mitchum, R.M., Vail, P.R., Sarg, J.F., Loutit, T.S., Hardenbol, J., 1988. An overview of the fundamentals of sequence stratigraphy and key definitions. In: Wilgus, C.K., Hastings, B.S., Kendall, C.G.St.C., Posamentier, H.W., Ross, C.A., Van Wagoner, J.C. (eds.). Sea level changes: an integrated approach. Society for Sedimentary Geology (SEPM), 42(Special Publication), 39-45.

Vail, P.R., Audemard, F., Bowman, S.A., Eisner, P.N., Perez-Cruz, C., 1991. The Stratigraphic Signatures of Tectonics, Eustasy and Sedimentology – an Overview. In: Einsele, G., Ricken, W., Seilacher, A. (eds.). Cycles and Events in Stratigraphy. Springer-Verlag Berlin Heidelberg 1991, 617-659.

Vennin, E., Aurell, M., 2001. Stratigraphie séquentielle de l'Aptien du sous-bassin de Galvé (Province de Teruel, NE de l'Espagne). Bulletin de la Société Géologique de France, 172, 397-410.

Vilas, L., Masse, J.P., Arias, C., 1995. *Orbitolina* episodes in carbonate platform evolution: the early Aptian model from SE Spain. Palaeogeography, Palaeoclimatology, Palaeoecology, 119, 35-45.

Vilas, L., Martín-Chivelet, J., Arias, C., 2003. Integration of subsidence and sequence stratigraphic analyses in the Cretaceous carbonate platforms of the Prebetic (Jumilla-Yecla Region), Spain. Palaeogeography, Palaeoclimatology, Palaeoecology, 200, 107-129.

Villanueva-Amadoz, U., Pons, D., Diez, J.B., Sender, L.M., Ferrer, J., 2008. Registro de granos de polen de angiospermas durante el Albiense-Cenomaniense en el NE de España. In: Ruiz-Omeñaca, J.I., Piñuela, L., García-Ramos, J.C. (eds.). Libro de resúmenes. Colunga, Museo del Jurásico de Asturias (MUJA), XXIV Jornadas de la Sociedad Española de Paleontología, 15-18 de octubre de 2008, 219-220.

Watts, A.B., 1981. The U.S. Atlantic continental margin: subsidence history, crustal structure and thermal evolution. In: Bally, A.W., Watts, A.B., Grow, J.A., Manspeizer, W., Bernoulli,

D., Schreiber, C., Hunt, J.M. (eds.). Geology of passive continental margins: history, structure and sedimentologic record (with special emphasis on the Atlantic margin). American Association of Petroleum Geologists (AAPG), Education Course Note Series, 19(2), 24pp.

Weisser, D., 1959. Acerca de la estratigrafía del Urgo-Aptense en las cadenas Celtibéricas de España. Notas y comunicaciones del Instituto Geológico y Minero de España, 55, 17-32.

Weissert, H., Lini, A., 1991. Ice age interludes during the time of Cretaceous greenhouse climate? In: Müller, D.W., McKenzie, J.A., Weissert, H. (eds.). Controversies in Modern Geology: Evolution of Geological Theories in Sedimentology, Earth History and Tectonics. Academic Press, 173-191.

Weissert, H., Lini, A., Föllmi, K.B., Kuhn, O., 1998. Correlation of Early Cretaceous carbon isotope stratigraphy and platform drowning events: a possible link? Palaeogeography, Palaeoclimatology, Palaeoecology, 137, 189-203.

Weissert, H., Erba, E., 2004. Volcanism, CO2 and palaeoclimate: a Late Jurassic-Early Cretaceous carbon and oxygen isotope record. Journal of the Geological Society, London, 161, 695-702.

Wissler, L., Funk, H., Weissert, H., 2003. Response of Early Cretaceous carbonate platforms to changes in atmospheric carbon dioxide levels. Palaeogeography, Palaeoclimatology, Palaeoecology, 200, 187-205.

Yose, L.A., Ruf, A.S., Strohmenger, C.J., Schuelke, J.S., Gombos, A., Al-Hosani, I., Al-Maskary, S., Bloch, G., Al-Mehairi, Y., Johnson, I.G., 2006. Three-dimensional characterization of a heterogeneous carbonate reservoir, Lower Cretaceous, Abu Dhabi (United Arab Emirates). In: Harris, P.M., Weber, L.J. (eds.). Giant hydrocarbon reservoirs of the world: From rocks to reservoir characterization and modeling. American Association of Petroleum Geologists (AAPG)/Society for Sedimentary Geology (SEPM), 88(Special Publication), 173-212.

Manuscript received July 2009;
revision accepted January 2010;
published Online May 2010.